

INTERFACIAL DROP DYNAMICS
IN A SIMPLE SHEAR FIELD

A Thesis
Presented to
the Faculty of the Department of Chemical Engineering
University of Houston

In Partial Fulfillment
of the Requirements for the Degree
Master of Science in Chemical Engineering

by
Robert W. Graves
August 1977

ACKNOWLEDGEMENTS

I wish to express my sincere gratitude to my advisor, Professor Raymond W. Flumerfelt, for his invaluable guidance, advice, and friendship throughout the course of this thesis research.

I am grateful to Mr. Roy M. Priest and Mr. David Wysocki of the Chemical Engineering Machine Shop for their assistance in constructing the experimental equipment; and Mr. Herb Kent of the Chemical Engineering Department for his kindly administrative assistance.

I am appreciative of the financial assistance from the Department of Chemical Engineering and from Texaco.

I also have heartfelt gratitude for my wife, Beth, for her assistance in some of the laboratory activities and for her typing of this thesis.

INTERFACIAL DROP DYNAMICS
IN A SIMPLE SHEAR FIELD

An Abstract of a Thesis
Presented to
the Faculty of the Department of Chemical Engineering
University of Houston

In Partial Fulfillment
of the Requirements for the Degree
Master of Science in Chemical Engineering

by
Robert W. Graves
August 1977

ABSTRACT

Dynamic interfacial phenomena were investigated by subjecting liquid drops to a simple shear field, which was generated by a Couette cylinder apparatus. Various studies of drop dynamics were carried out, including deformation tests, the position of the critical streamline (external to the drop), and the period of circulation around internal streamlines.

Significant dynamic interfacial behavior was observed in a liquid-liquid system that contained no added surfactant. Drops behaved much like rigid bodies in the internal circulation and the critical streamline experiments. Very large effects were caused by either the interfacial dilational viscosity (κ) or by interfacial tension gradients, which have similar effects as κ . The interfacial shear viscosity (ϵ) was also observed, but to a lesser degree. Values for these effects were about 3.33 surface poise for the κ -type effects, and 0.18 surface poise for the ϵ effect. Trace impurities that acted as surfactants may have been responsible for these results.

Dynamic interfacial behavior, though smaller in magnitude, was also observed in a surfactant, low interfacial tension system, which was intended to somewhat resemble the liquids encountered in micellar chemical flooding. High concentrations of the surfactant were used to reduce the possibility of developing interfacial tension gradients. Effects caused by either the interfacial dilational viscosity or interfacial tension gradients were apparently negligible, whereas the interfacial shear viscosity appeared to be in the range of 0.03 to 0.21 surface poise.

The potential of very small surfactant concentrations to cause

significant dynamic interfacial behavior was demonstrated. Trace impurities that act as surfactants, for example, could induce these effects by creating large interfacial tension gradients. Conversely, high concentrations of surfactant would decrease the chances of such effects occurring.

TABLE OF CONTENTS

1	INTRODUCTION	1
1.1	Background On Dynamic Interfacial Phenomena	1
1.2	Applications	3
1.3	Objectives	3
2	THEORETICAL BACKGROUND	5
2.1	General Theory	5
2.2	Drop Deformation	11
2.3	Internal Circulation and the Critical Streamline	21
3	EXPERIMENTAL STUDIES	29
3.1	Experimental Apparatus.	29
3.2	Experimental Procedures	32
3.3	Materials and Physical Properties	37
4	RESULTS AND DISCUSSIONS	43
4.1	General Data Analysis	43
4.2	System A Results.	45
4.3	System B Results.	58
5	CONCLUSIONS AND RECOMMENDATIONS.	74
	BIBLIOGRAPHY.	78
	APPENDIX I Experimental Data	79
	APPENDIX II Error Analysis	92
	NOMENCLATURE	94

LIST OF FIGURES

2.1-1	Drop in a Simple Shear Field.	6
2.1-2	Geometry of Drop in a Shear Field	7
2.3-1	Circulation Times Inside Drop for Various Values of λ and r_0	23
2.3-2	Positions of Drop Critical Streamlines for Various Values of λ	24
3.1-1	Schematic of the Experimental Apparatus	30
3.1-2	Photograph of the Experimental Apparatus.	31
3.2-1	Typical Drop Deformation Sequence (System B).	34
4.2-1	Time Dependence of Deformation: System A	46
4.2-2	Deformation Data (D/N_G) and Fitted Curve: System A . . .	48
4.2-3	Deformation Data (λR) and Fitted Curve: System A	49
4.2-4	Deformations (D/N_G) for Various Values of κ/ϵ : System A	50
4.2-5	Values of λR , from Drop Deformations, for Various Values of κ/ϵ : System A	51
4.2-6	Data of γ_{eff}/γ from Drop Deformations: System A	52
4.2-7	Experimental Internal Circulation Times and Fitted Curve: System A	54
4.2-8	Experimental Critical Streamline Position and Fitted Curve: System A	55
4.3-1	Dependence of Interfacial Tension on Surfactant Concen- tration: System B	59
4.3-2	Effect of N_{gv} on Deformation Data: System B	60
4.3-3	Time Dependence of Deformation: System B	61
4.3-4	Effect of N_G on Deformation Data: System B	62
4.3-5	Deformation Data (D/N_G) and Fitted Curve: System B . . .	64
4.3-6	Deformation Data (λR) and Fitted Curve: System B	65
4.3-7	Deformations (D/N_G) for Various Values of ϵ/κ : System B.	66

4.3-8	Values of λR , from Drop Deformations, for Various Values of $\kappa+\epsilon$: System B	67
4.3-9	Data of $\gamma_{\text{eff}}/\gamma$ from Drop Deformations: System B	70
4.3-10	Experimental Internal Circulation Times and Fitted Curve: System B	71

LIST OF TABLES

2.2-1	Sensitivity of D and α To Small Values of N_G	18
3.3-1	Physical Properties of Materials	41
1-1	Deformation Data for System A.	80
1-2	Internal Circulation Data for System A	84
1-3	Critical Streamline Data for System A	84
1-4	Deformation Data for System B	86
1-5	Internal Circulation Data for System B	90
1-6	Interfacial Tension for System B	91
11-1	Summary of Data Errors	93

CHAPTER I

INTRODUCTION

1.1 Background On Dynamic Interfacial Phenomena

The interfacial region between two homogeneous phases exhibits properties different from those in either of the bulk phases. The property of the interfacial tension is used to describe the forces acting on an interface when two phases come into contact with each other.

A moving interface, as opposed to a static one, cannot be described in terms of interfacial tension alone; additional properties are required to describe the viscous and elastic forces and interfacial tension gradients acting on the interface. A fluid-fluid interface can deform in a number of ways when moving, such as dilation, shear, bending, and torsion. Viscosities and elasticities have been attributed to each of these by Boussinesq (2), who modelled the interface by its interfacial tension, an interfacial shear viscosity, and an interfacial dilational viscosity; and by Oldroyd (8), who suggested that elastic properties be included.

An interface offering resistance to all of these deformations would be visco-elastic, or non-Newtonian. The resistances to bending and torsion are usually not considered, since they would probably be important only when the interfacial region is relatively thick. With this consideration, a normal and tangential stress balance on the interface (7) would include the following terms:

1. Interfacial tension
2. Gradient of interfacial tension
3. Dilational viscosity

4. Dilational elasticity
5. Shear viscosity
6. Shear elasticity

In this study only the interfacial tension (γ), interfacial tension gradients ($\text{grad } \gamma$), interfacial dilational viscosity (κ), and interfacial shear viscosity (ε) are considered, which is a Newtonian rheological model of the interface.

Surface active agents, or surfactants, can radically alter both the static and dynamic behavior of an interface. Their adsorption at the interface changes the nature of the interfacial region. The two phases become more cohesive toward each other, which results in a lowering of the interfacial tension, for instance. An addition of surfactants, which alters the ability of an interface to resist various deformations, will also show up as a change in the viscous and elastic interfacial properties.

When the interface flows and deforms, the concentration of surfactant on it changes as the interface stretches and contracts. An interface that deforms unevenly (one area stretches while a different area contracts) will have spatial variations of surfactant concentration on it, if the deformations are faster than the time required for the surfactant molecules to redistribute themselves evenly over the interface. Since the interfacial tension is a function of the concentration of surfactant, these variations of concentration on the interface will produce interfacial tension gradients. As already mentioned, gradients in the interfacial tension give rise to stress differences across the interface, which alter the flow and deformation of the interface.

1.2 Applications

By altering the ability of an interface to deform, dynamic interfacial properties also affect the velocity distribution in the immediate neighborhood of the interface. These parameters, then, can be expected to be most important in physical or chemical processes dealing with the interface itself or where the surface area to volume ratio is high.

Several topic areas come to mind, such as the stability of foams and emulsions, or mass transfer operations, like gas absorption, distillation, and liquid extraction. The dynamic properties may also be significant in the displacement and recovery of residual oil (12) employing surfactant solutions (micellar chemical flooding techniques of enhanced oil recovery).

1.3 Objectives

The general objective of this work is to study interfacial behavior by observing small drops placed in a shear field. This general objective can be broken into two main parts:

1. To investigate dynamic interfacial phenomena by subjecting drops to a simple shear field that is generated by a Couette cylinder apparatus. Deformation studies of drops are to be made, as well as the position of the critical streamline external to the drop and the circulation periods around internal streamlines. These studies will consider effects caused by interfacial tension gradients ($\text{grad } \gamma$) and interfacial dilational and shear viscosities (κ and ϵ). There are few reliable methods at present to investigate these properties, particularly the dilational viscosity.

2. To find the relative magnitudes of the individual properties in two particular liquid-liquid systems. One will be a high interfacial tension system with no surfactants added, and the other will be a surfactant, low interfacial tension system, which will somewhat resemble those used in micellar chemical floods.

CHAPTER 2

THEORETICAL BACKGROUND

2.1 General Theory

Previous analyses of drop dynamics in shear fields have not taken into account dynamic interfacial effects such as interfacial tension gradients or interfacial viscous and elastic properties. Interfacial tension alone was used to describe the pressure difference across the interface.

The problem being considered is what the dynamics of a liquid drop will be when placed in another immiscible liquid undergoing simple shear, namely

$$V_x = 0, V_y = Gx, V_z = 0 \quad (2.1-1)$$

where G is the shear rate of the undisturbed flow field. As the shear rate is increased, the pressure and viscous stresses at the interface will deform the drop from its original spherical shape. Refer to Figures 2.1-1 and 2.1-2 for the geometry of the drop in the shear field.

One of the first to analyze the drop's deformation was Taylor (16, 17), who solved this problem using the following assumptions and boundary conditions:

1. Steady, incompressible flow
2. Newtonian fluids
3. Inertial effects small compared to viscous effects
4. Gravitational effects small compared to viscous shear effects (neutrally buoyant drop)
5. Continuity of tangential velocity components
6. Continuity of tangential stress

DROP IN SIMPLE SHEAR FIELD

$$D = \text{DEFORMATION} = \frac{L - B}{L + B}$$

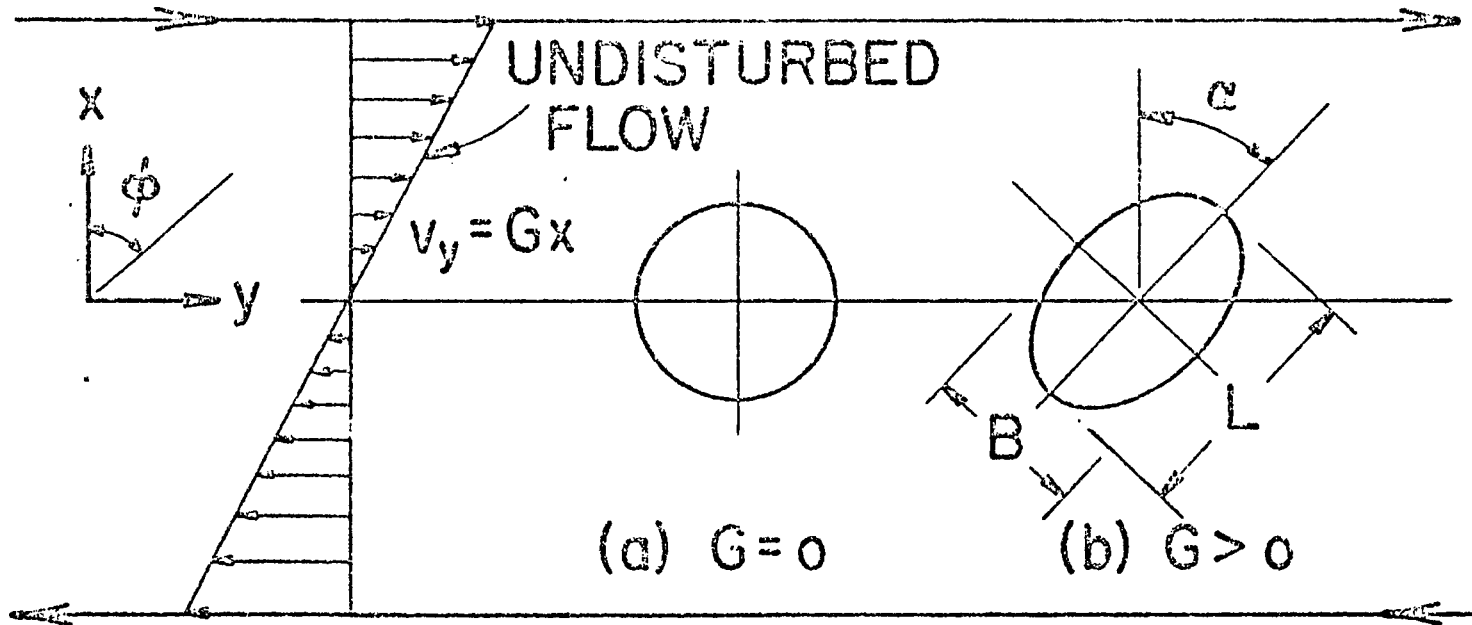
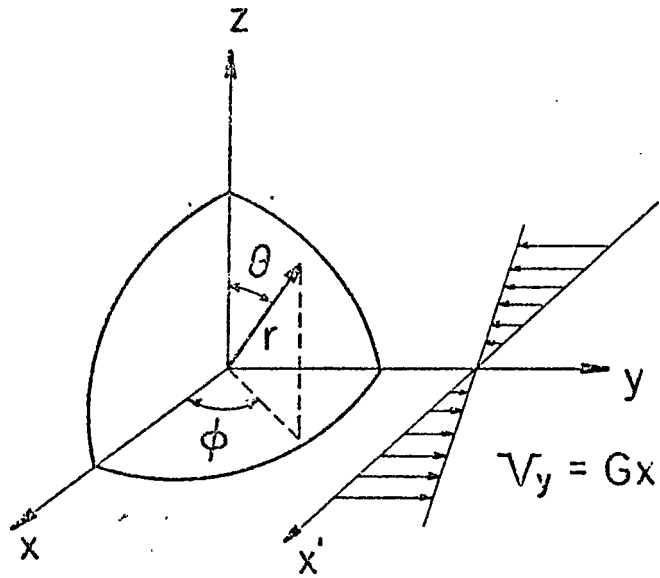
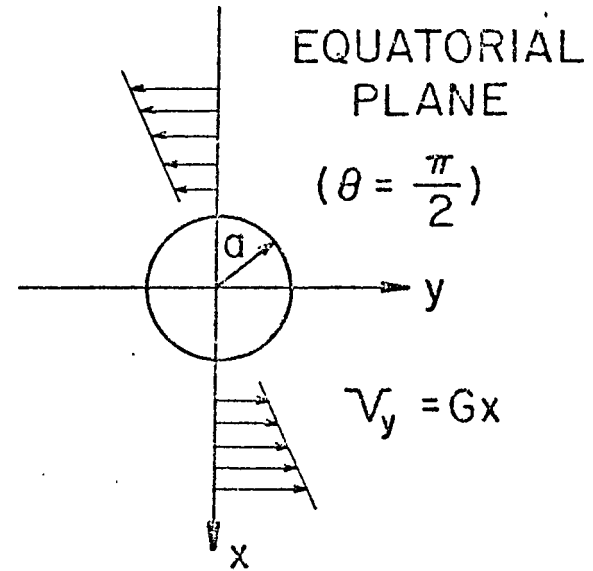


Figure 2.1-1. Drop in a Simple Shear Field

GEOMETRY



(a)



(b)

Figure 2.1-2. Geometry of Drop in a Shear Field

7. Normal stresses balanced by interfacial tension

He obtained limiting case solutions for the velocity field in terms of the viscosity ratio (N_μ) and a dimensionless capillary number (N_G). The viscosity ratio is represented by

$$N_\mu = \frac{\hat{\mu}}{\mu} \quad (2.1-2)$$

(the drop phase viscosity to the continuous phase viscosity), and the capillary number by

$$N_G = \frac{\mu G a}{\gamma} \quad (2.1-3)$$

where "a" is the undisturbed drop radius. A ^ over a variable will be used to denote the drop phase. Taylor then characterized the drop deformation by a normalized deformation measure defined by

$$D = \frac{(L - B)}{(L + B)} \quad (2.1-4)$$

and the drop orientation by an angle α . Here, L and B are the major and minor axes of the deformed drop (See Figures 2.1-1 and 2.1-2). The limiting case results were:

1. As $N_G \rightarrow 0$

$$D = N_G \frac{(19N_\mu + 16)}{(16N_\mu + 16)}, \quad \alpha = \frac{\pi}{4} \quad (2.1-5)$$

2. As $N_\mu \rightarrow \infty$

$$D = \frac{5}{4} N_\mu, \quad \alpha = \frac{\pi}{2} \quad (2.1-6)$$

Further analyses were done to determine the streamlines and circulation times inside and outside a spherical drop, again assuming no dynamic interfacial properties. The results are given by Torza, Henry, Cox, and Mason (18), who used the previously stated boundary conditions.

Several investigators (10, 15) have noted some disagreement between the theoretical predictions above and experimental observations on drop dynamics. These discrepancies can be explained by the existence of contaminants or surfactants which alter the nature of the interface, and thus invalidate the interfacial boundary conditions used in obtaining the results in Equations (2.1-5) and (2.1-6). A method that incorporates κ , ϵ , and $\text{grad } \gamma$ effects into more general boundary conditions is required when analyzing drop dynamics.

Wei, Schmidt, and Slattery (19) assumed a Newtonian surface fluid model for the surface stress tensor, which includes γ , κ , and ϵ . Then they used a perturbation analysis to find the velocity field to the first order in the perturbation parameter N_G . The analysis enabled them to determine the combination $(3\kappa + 2\epsilon)$ from the experimental measurement of circulation times at the drop interface. No effort was made to determine the drop deformation from this model.

The boundary conditions used by these investigators at the drop interface were (replacing Taylor's boundary conditions Nos. 6 and 7):

6. Normal velocity components satisfy the jump mass balance (11, 14)

$$\text{div}_{(\sigma)} (\rho^{(\sigma)} \underline{v}^{(\sigma)}) + \rho \underline{v} \cdot \underline{\xi} - \hat{\rho} \hat{\underline{v}} \cdot \underline{\xi} = 0 \quad (2.1-7)$$

where $\rho^{(\sigma)}$ is the interfacial mass density, $\underline{v}^{(\sigma)}$ the interfacial velocity, and $\underline{\xi}$ the unit normal to the interface pointing into the continuous phase.

7. Discontinuity of bulk phase stresses described by the jump momentum balance (11, 14, 13)

$$\text{grad}_{(\sigma)} \gamma + \text{div}_{(\sigma)} \underline{\underline{S}}^{(\sigma)} + 2H \gamma \underline{\xi} + \rho^{(\sigma)} \underline{b} + \underline{T} \cdot \underline{\xi} - \hat{\underline{T}} \cdot \underline{\xi} = 0 \quad (2.1-8)$$

The last four terms represent the standard boundary condition, where $\rho^{(\sigma)} \underline{b}$ is the body force acting on the interface, and $2H\gamma \underline{\xi}$ is the normal force at the interface caused by γ , H being the mean curvature. Also, $\underline{\tau} \cdot \underline{\xi}$ and $\hat{\underline{\tau}} \cdot \underline{\xi}$ are the bulk phase forces (normal and tangential) acting on the interface, where $\underline{\tau}$ and $\hat{\underline{\tau}}$ are the stress tensors for the bulk phases. The first two terms of Equation (2.1-8) represent the dynamic interfacial effects. $\text{grad}_{(\sigma)} \gamma$ represents forces tangent to the interface from gradients of γ , and $\text{div}_{(\sigma)} \underline{S}^{(\sigma)}$ represents interfacial forces from the resistance of the interface to being deformed. Here $\underline{S}^{(\sigma)}$ is the viscous portion of the interfacial stress tensor, which for a Newtonian interfacial fluid model (11, 14) is given by

$$\underline{S}^{(\sigma)} = (\kappa - \epsilon) (\text{div}_{(\sigma)} \underline{v}^{(\sigma)}) \underline{P} + \epsilon [\underline{P} \cdot \nabla_{(\sigma)} \underline{v}^{(\sigma)} + (\nabla_{(\sigma)} \underline{v}^{(\sigma)})^+ \cdot \underline{P}] \quad (2.1-9)$$

where P is the projection tensor that transforms any vector on the interface into its tangential component.

Wei, et al. considered the case where at least one surfactant (A) was present in the system. They then assumed:

8. The interfacial properties (γ , κ , ϵ , and $\rho^{(\sigma)}$) are functions of the interfacial mass density of A ($\rho_A^{(\sigma)}$).
9. The jump mass balance of A at the interface (13) is described by

$$\begin{aligned} \text{div}_{(\sigma)} (\rho_A^{(\sigma)} \underline{v}^{(\sigma)}) + \text{div}_{(\sigma)} \underline{j}_A^{(\sigma)} + \rho_A \underline{v} \cdot \underline{\xi} \\ - \rho_A \underline{v} \cdot \underline{\xi} + \underline{j}_A \cdot \underline{\xi} - \hat{\underline{j}}_A \cdot \underline{\xi} = 0 \end{aligned} \quad (2.1-10)$$

where $\underline{j}_A^{(\sigma)}$, \underline{j}_A , and $\hat{\underline{j}}_A$ represent diffusive mass fluxes of

A in the interface, continuous phase and drop phase, respectively.

10. The equations of continuity of A in the continuous and drop phases, respectively, are given by

$$\operatorname{div}(\rho_A \underline{v}) + \operatorname{div} \underline{j}_A = 0 \quad (2.1-11)$$

$$\operatorname{div}(\hat{\rho}_A \hat{\underline{v}}) + \operatorname{div} \hat{\underline{j}}_A = 0 \quad (2.1-12)$$

When Wei, et al. applied these new conditions to the bulk phase continuity and momentum equations in a Taylor type analysis, they obtained the velocity fields inside and outside the drop to the order N_G . This analysis was then continued to determine the circulation time at the interface of a drop in terms of the combination $(3\kappa+2\varepsilon)$ and N_μ .

2.2 Drop Deformation

The previous analysis has been extended by Flumerfelt (4, 5) to determine the shape of the drop and its orientation angle. The results are quite different from those predicted by Taylor.

Flumerfelt's first analysis (5) assumed no mass transfer effects or interfacial tension gradients, as did Wei, et al. He obtained the following expression for deformations to the first order in N_G

$$\frac{D}{N_G} = \frac{5 (24N_\kappa + 8N_\varepsilon + 19N_\mu + 16)}{16 (6N_\kappa + 4N_\varepsilon + 5N_\mu + 5)} \quad (2.2-1)$$

where

$$N_\kappa = \frac{\kappa}{\mu a} \quad (2.2-2)$$

$$N_\varepsilon = \frac{\varepsilon}{\mu a} \quad (2.2-3)$$

The predicted value for the orientation angle for the first order perturbation analysis on N_G was $\alpha = \pi/4$, the same as Taylor's theory.

Some limiting cases for D/N_G follow.

1. As $N_K, N_\epsilon \rightarrow 0$

$$\frac{D}{N_G} = \frac{19N_\mu + 16}{16N_\mu + 16} \quad (2.2-4)$$

This is Taylor's result, which would hold either when the interfacial viscous effects are very small, or for very large drops (as " a " $\rightarrow \infty$, $N_K, N_\epsilon \rightarrow 0$). Note that D/N_G is bounded between 1 and 19/16.

2. As $N_K, N_\epsilon \rightarrow \infty$

$$\frac{D}{N_G} = \frac{5(3N_K + N_\epsilon)}{4(3N_K + 2N_\epsilon)} \quad (2.2-5)$$

This would apply when interfacial viscous effects dominate the bulk viscous effects, or when the drops are very small (as " a " $\rightarrow 0$, $N_K, N_\epsilon \rightarrow \infty$).

3. As $N_K \rightarrow \infty$

$$\frac{D}{N_G} = \frac{5}{4} \quad (2.2-6)$$

When the interfacial dilational viscosity dominates, the deformation is enhanced.

4. As $N_\epsilon \rightarrow \infty$

$$\frac{D}{N_G} = \frac{5}{8} \quad (2.2-7)$$

When the interfacial dilational shear viscosity dominates, the deformation is inhibited.

If experiments are run to measure the drop deformation at various shear rates, κ and ϵ cannot be found independently of each other. Rather, only general effects of κ and ϵ can be found if D/N_G is less than 1 or greater than 19/16. If D/N_G were found to lie within this range, no valid conclusions could be drawn since κ and ϵ could balance each other's effect on D/N_G , or they may not exist at all. Independent measurements of κ and ϵ would be required to determine the other variables.

Flumerfelt further extended this analysis to include mass transfer of surfactant molecules (4). For this case he obtained the following expression for deformations to the first order in N_G

$$\frac{D}{N_G} = \frac{5 (24N_\kappa + 8N_\epsilon + 19N_\mu + 16 + 24N_\sigma)}{16 (6N_\kappa + 4N_\epsilon + 5N_\mu + 5 + 6N_\sigma)}, \quad \alpha = \frac{\pi}{4} \quad (2.2-8)$$

The additional term N_σ represents the mass transfer of surfactant. The expression for N_σ will not be given here, but in general it is inversely proportional to the diffusion coefficient of surfactant on the interface and the diffusion coefficients in the continuous and drop phases, and it is directly proportional to $(d\gamma/d \ln c_s)$. The term $(d\gamma/d \ln c_s)$ is the variation of interfacial tension with the logarithmic concentration of surfactant (c_s) in the fluid systems. In many systems, the curve for γ as a function of c_s is steep at low c_s and flattens out as more surfactant is added to the system. When the concentration of surfactant is high in such systems, $(d\gamma/d \ln c_s)$ will usually be small and thus make N_σ small. Also, if the diffusion coefficients for the surfactant are large, then N_σ will inversely be small.

When the concentration of added surfactant is very small, or when trace impurities in the fluids act as surfactants, the value of $(d\gamma/d \ln c_s)$

will become very large, consequently making N_{σ} very large. The reasoning behind this effect can be explained by considering the dilation of the drop's interface. As surfactant molecules travel across the drop, the interface compresses over one quadrant and then expands as it moves across the next quadrant of the interface. When these variations of area occur, the surfactant concentration changes from point to point. The surfactant molecules seek to bring their concentration over the entire surface to a constant value by diffusion across the interface or by absorbing and desorbing with molecules in the bulk liquids. If the concentration of molecules in the bulk is small, the time required for them to exchange molecules with the interface is lengthened. And if the time required for the surfactant to establish an equilibrium concentration over the interface is longer than the time of expansion or compression of the interface, interfacial tension gradients will develop. This explains how trace impurities can result in large values of N_{σ} . This also suggests that interfacial tension gradients would appear as dilational effects in the drop interfacial behavior.

Briefly then, N_{σ} describes the likelihood that interfacial tension gradients will develop over the drop's interface. If the bulk phase concentration of surfactant molecules is high and/or their rates of diffusion are fast, then the chances of interfacial tension gradients developing would be very small. Gradients could be expected, on the other hand, if the surfactant concentration is small or diffuses very slowly.

The limits of N_{σ} in Equation (2.2-8) are worth noting:

1. As $N_{\sigma} \rightarrow 0$

$$\frac{D}{N_G} = \frac{5 (24N_K + 8N_\epsilon + 19N_\mu + 16)}{16 (6N_K + 4N_\epsilon + 5N_\mu + 5)} \quad (2.2-9)$$

This is the same result obtained (see Equation (2.2-1)) when mass transfer effects were considered to be negligible.

2. As $N_{\mathcal{D}} \rightarrow \infty$

$$\frac{D}{N_G} = \frac{5}{4} \quad (2.2-10)$$

This is the same limit obtained for $N_K \rightarrow \infty$.

The effect of $N_{\mathcal{D}}$ on D/N_G is the same as that of N_K , which was suggested in the previous discussion. If $N_{\mathcal{D}}$ or N_K cannot be determined by some other method, then deformation experiments could not distinguish between the two variables. For this reason a new variable will be introduced to represent the effect of either N_K or $N_{\mathcal{D}}$:

$$N_{K+\mathcal{D}} = N_K + N_{\mathcal{D}} \quad (2.2-11)$$

With this substitution, Equation (2.2-8) becomes

$$\frac{D}{N_G} = \frac{5 (24N_{K+\mathcal{D}} + 8N_\epsilon + 19N_\mu + 16)}{16 (6N_{K+\mathcal{D}} + 4N_\epsilon + 5N_\mu + 5)} \quad (2.2-12)$$

which is similar in form to the earlier derived Equation (2.2-1). Once again, deformation experiments alone could not determine the individual terms for $N_{K+\mathcal{D}}$ or N_ϵ . At best, this equation could be used to give the relative magnitudes of the two effects by noting if D/N_G was outside the range of 1 and 19/16.

Flumerfelt more recently (5) has followed the approach of Cox (3) and obtained a small deformation theory valid over a full range of N_G values. It assumes mass transfer effects are negligible, however. The expressions obtained for small deformations are

$$D = \frac{5}{4} \frac{(19\lambda + 16) + \lambda(\kappa' - 9\epsilon')}{(\lambda + 1) [(20/N_G)^2 + (19\lambda R)^2]^{\frac{1}{2}}} \quad (2.2-13)$$

$$\alpha = \frac{\pi}{4} + \frac{1}{2} \tan^{-1} (19N_G \lambda R / 20) \quad (2.2-14)$$

where

$$\lambda = N_\mu + \frac{2}{5} (3N_\kappa + 2N_\epsilon) \quad (2.2-15)$$

$$\kappa' = \frac{6}{5} \frac{N_\kappa}{\lambda} \quad (2.2-16)$$

$$\epsilon' = \frac{4}{5} \frac{N_\epsilon}{\lambda} \quad (2.2-17)$$

$$R = 1 - \frac{1}{114} [113\kappa' + 33\epsilon' + (\kappa' - 9\epsilon')^2] \quad (2.2-18)$$

$$\lambda R = \lambda - \frac{\lambda}{114} [113\kappa' + 33\epsilon' + (\kappa' - 9\epsilon')^2] \quad (2.2-19)$$

Some limiting cases follow:

1. As $N_G \rightarrow 0$

$$D = \frac{5}{4} \frac{1}{20/N_G} \frac{(19\lambda + 16) + \lambda(\kappa' - 9\epsilon')}{(\lambda + 1)} \quad (2.2-20)$$

which upon simplification becomes

$$\frac{D}{N_G} = \frac{5 (24N_\kappa + 8N_\epsilon + 19N_\mu + 16)}{16 (6N_\kappa + 4N_\epsilon + 5N_\mu + 5)} \quad (2.2-21)$$

This once again is Equation (2.2-1). The limit for the orientation angle is

$$\alpha = \frac{\pi}{4} \quad (2.2-22)$$

which agrees with the previous analyses for small N_G .

2. As $\kappa, \epsilon \rightarrow 0$

$$\lambda = N_{\mu}, R = 1, \lambda R = N_{\mu} \quad (2.2-23)$$

$$D = \frac{5}{4} \frac{(19N_{\mu} + 16)}{(N_{\mu} + 1) [(20/N_G)^2 + (19N_{\mu})^2]^{\frac{1}{2}}} \quad (2.2-24)$$

$$\alpha = \frac{\pi}{4} + \frac{1}{2} \tan^{-1} (19N_G N_{\mu}/20) \quad (2.2-25)$$

3. As $\lambda \rightarrow \infty$ or $(19\lambda R)^2 \gg (20/N_G)^2$

$$D = \frac{5}{4\lambda R} + \frac{5(\kappa' - 9\epsilon')}{76\lambda R} \quad (2.2-26)$$

$$\alpha = \frac{\pi}{2} \quad (2.2-27)$$

This could occur either when $\lambda \rightarrow \infty$, or N_G and $\lambda R > 1$.

The limiting case for small N_G , (No. 1), is misleading when compared to the previous result (Equation (2.2-1)) which was based on a perturbation of the parameter N_G . Although Equation (2.2-21) is a good approximation for calculating D when N_G is small, Equation (2.2-22) is generally not a good approximation for α . To state this briefly, α is much more sensitive to small N_G than D . Table 2.2-1 gives an indication of this effect. Values for D can be calculated reasonably accurately by Equation (2.2-21) for $N_G = 0.3$ and $\lambda R \leq 1$, and even when $N_G = 0.1$ and $\lambda R = 5$ the deformation can be found with less than 10% error.

These more recent expressions, of the last two pages, provide a good basis to use when deformation experiments are run to investigate the interfacial dynamic properties. In addition to being valid for all N_G , Equations (2.2-13) and (2.2-14) can be used to evaluate κ and ϵ individually, which earlier expressions for D could not do.

As the equations stand now, both are functions of N_{κ} , N_{ϵ} , and N_G ,

Table 2.2-1

Sensitivity of D and α to Small Values of N_G

Conditions	D Calculated from Eq. (2.2-13)	α Calculated from Eq. (2.2-14)
	D Calculated from Eq. (2.2-21)	α Calculated from Eq. (2.2-22)
$\lambda R = 1$ $N_G = 0.1$	0.996	1.060
$\lambda R = 1$ $N_G = 0.3$	0.962	1.177
$\lambda R = 5$ $N_G = 0.1$	0.903	1.282

or κ , ϵ , G , and "a". Taking out the dependence on N_G (or G) would facilitate analysis of the data. A variable that is not dependent on N_G would be desirable, such as λR . Equation (2.2-14) can be rearranged into the form

$$\lambda R = \frac{20}{19N_G} \tan \left[2 \left(\alpha - \frac{\pi}{4} \right) \right] \quad (2.2-28)$$

This equation can be used to obtain λR experimentally from α and N_G data. The experimental values of λR can then be used in Equation (2.2-19), which is a function of κ , ϵ , and "a".

Equation (2.2-13) cannot be transformed into such a convenient form, however. An alternative is to use Equations (2.2-21) or (2.2-26) in place of Equation (2.2-13) when the limits used to obtain the first two equations from the latter one are applicable. Note that the left-hand side of either Equation (2.2-21) or (2.2-26) is only a function of κ , ϵ , and "a".

Equations (2.2-13) and (2.2-19) provide a way to calculate κ and ϵ from D , N_G , and λR data on various sized drops. The only restrictions are that the deformation D must be small and there are no interfacial tension gradients. When conditions are such that Equations (2.2-21) and (2.2-26) are valid, the calculations are easier since both λR and D/N_G (or D as the case may be) are only functions of κ , ϵ , and "a", and they are independent of N_G .

The effects of mass transfer can be included if N_K is changed to

$$N_{\kappa+\sigma} = N_K + N_\sigma \quad (2.2-11)$$

All expressions containing N_K would consequently be altered to contain $N_{\kappa+\sigma}$ terms, such as the two following expressions:

$$\kappa' = \frac{6}{5} \frac{N_{\kappa+\sigma}}{\lambda} \quad (2.2-29)$$

$$\lambda = N_{\mu} + \frac{2}{5} (3N_{\kappa} + 2N_{\epsilon}) \quad (2.2-30)$$

The proposed substitutions for N_{κ} in this particular analysis have not been rigorously proven. They are inferred, however, from the analysis that took mass transfer effects into account, resulting with Equation (2.2-8).

A different approach to account for the interfacial dynamic forces is to look at their net effect and not be concerned with their individual contributions. Since Taylor's result includes no interfacial dynamic effects, let a function $f(\lambda)$ include all of these effects so that the deformation is represented by

$$\frac{D}{N_G} = f(\lambda) \frac{(19N_{\mu} + 16)}{(16N_{\mu} + 16)} \quad (2.2-31)$$

Substitution of $\mu Ga/\gamma$ for N_G and rearrangement gives

$$\frac{\gamma}{f(\lambda)} = \frac{\mu Ga}{D} \frac{(19N_{\mu} + 16)}{(16N_{\mu} + 16)} \quad (2.2-32)$$

We now define a pseudo interfacial tension as $\gamma/f(\lambda)$ and call it the "effective interfacial tension"

$$\gamma_{\text{eff}} = \frac{\gamma}{f(\lambda)} \quad (2.2-33)$$

Substitution of this expression into Equation (2.2-32) and rearrangement yields

$$\frac{\gamma_{\text{eff}}}{\gamma} = \frac{1}{D/N_G} \frac{(19N_{\mu} + 16)}{(16N_{\mu} + 16)} \quad (2.2-34)$$

This equation is a convenient way to illustrate the effects of dynamic interfacial effects on the deformation of drops in shear fields. The term γ_{eff} must not be misconstrued to mean a new value for γ when dy-

dynamic forces are present. It merely gives an indication of the sizes of the forces and their effect on the deformation.

2.3 Internal Circulation and the Critical Streamline

The streamlines and circulation times inside and outside of the drop provide another method of studying interfacial phenomena. As stated in Section 2.1, the streamline and circulation equations were derived by Torza, Henry, Cox and Mason (18) for undeformed drops. In this study, dynamic interfacial effects were not considered. An equation was also obtained that described the critical streamline outside the drop, which separated regions of closed and open streamlines. The equations for times of circulation outside the drop were therefore only applicable on the closed streamlines inside the critical region. All of these equations were shown to be dependent on the viscosity ratio of the drop phase to the continuous phase (N_μ).

Fortunately, the velocity field obtained when dynamic interfacial effects are considered (as analyzed by Wei, Schmidt, and Slattery (19)) is identical to the velocity field of Torza, et al., if the N_μ parameter in their paper is interpreted as

$$\lambda = N_\mu + \frac{2}{5} (3N_\kappa + 2N_\epsilon) \quad (2.2-15)$$

Therefore, all of the circulation and streamline results of Torza, et al. are usable for dynamic interfacial effects when N_μ is reinterpreted as λ .

The period of circulation T on any particular streamline in the equatorial plane ($\theta = \frac{\pi}{2}$) can be nondimensionalized in terms of a circulation number

$$m = \frac{TG}{4\pi} \quad (2.3-1)$$

This is a function of λ and r_0 , where r_0 is the dimensionless radial position of the streamline at $\phi = 0$. The equations derived for circulation times internal and external to the drop each take on a different form, but both are in terms of an integral and must be solved numerically. Figure 2.3-1 shows the dependence of m on λ at various r_0 for internal circulation. (See Phillips (9) for computational details.) The period of circulation on the drop's surface can be found explicitly as

$$m \Big|_{\frac{r}{a} = 1} = \frac{\lambda + 1}{[\lambda(\lambda + 2)]^{\frac{1}{2}}} \quad (2.3-2)$$

The equations for internal and external streamlines in the equatorial plane are in terms of λ , r_0 and their positions (r , ϕ for spherical coordinates). The internal and external streamline equations are each of different forms, and both can be solved only by numerical methods. Figure 2.3-2 shows the positions of the critical streamline for various λ . Streamlines inside this region are closed, and ones outside the region are open.

Five different measurements can be envisioned to study dynamic interfacial phenomenon using drop circulation experiments in shear fields:

1. Circulation times on streamlines inside the drop
2. Circulation times on the drop's surface
3. Circulation times on streamlines inside the critical streamline, outside of the drop
4. Paths of streamlines inside the drop
5. Paths of streamlines outside the drop

For circulation time experiments, tracer particles on closed streamlines can be used to find the period of circulation T (and thus m) at a particular value of r_0 . The various circulation equations can then be

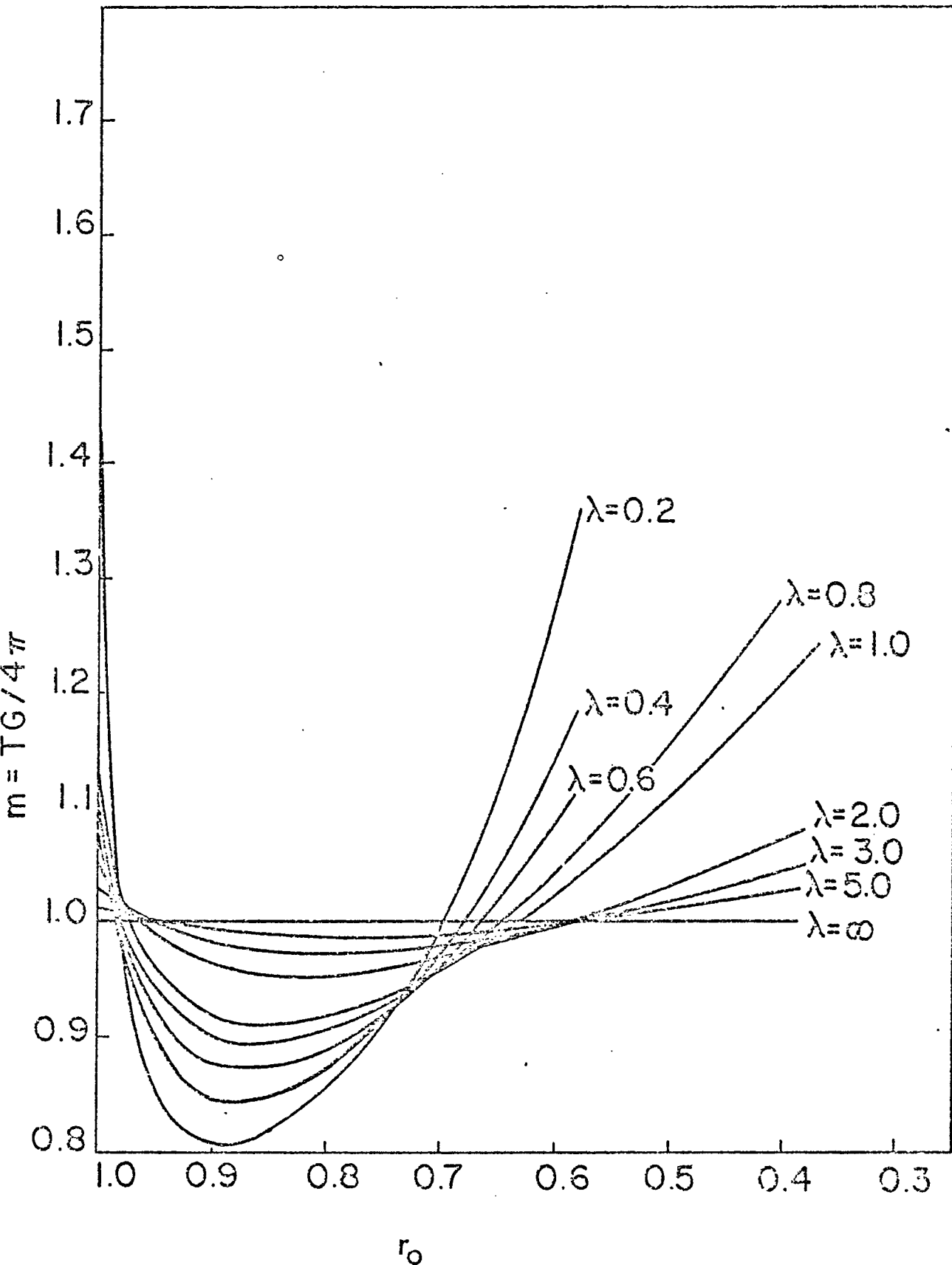


Figure 2.3-1. Circulation Times inside Drop for Various Values of λ and r_0

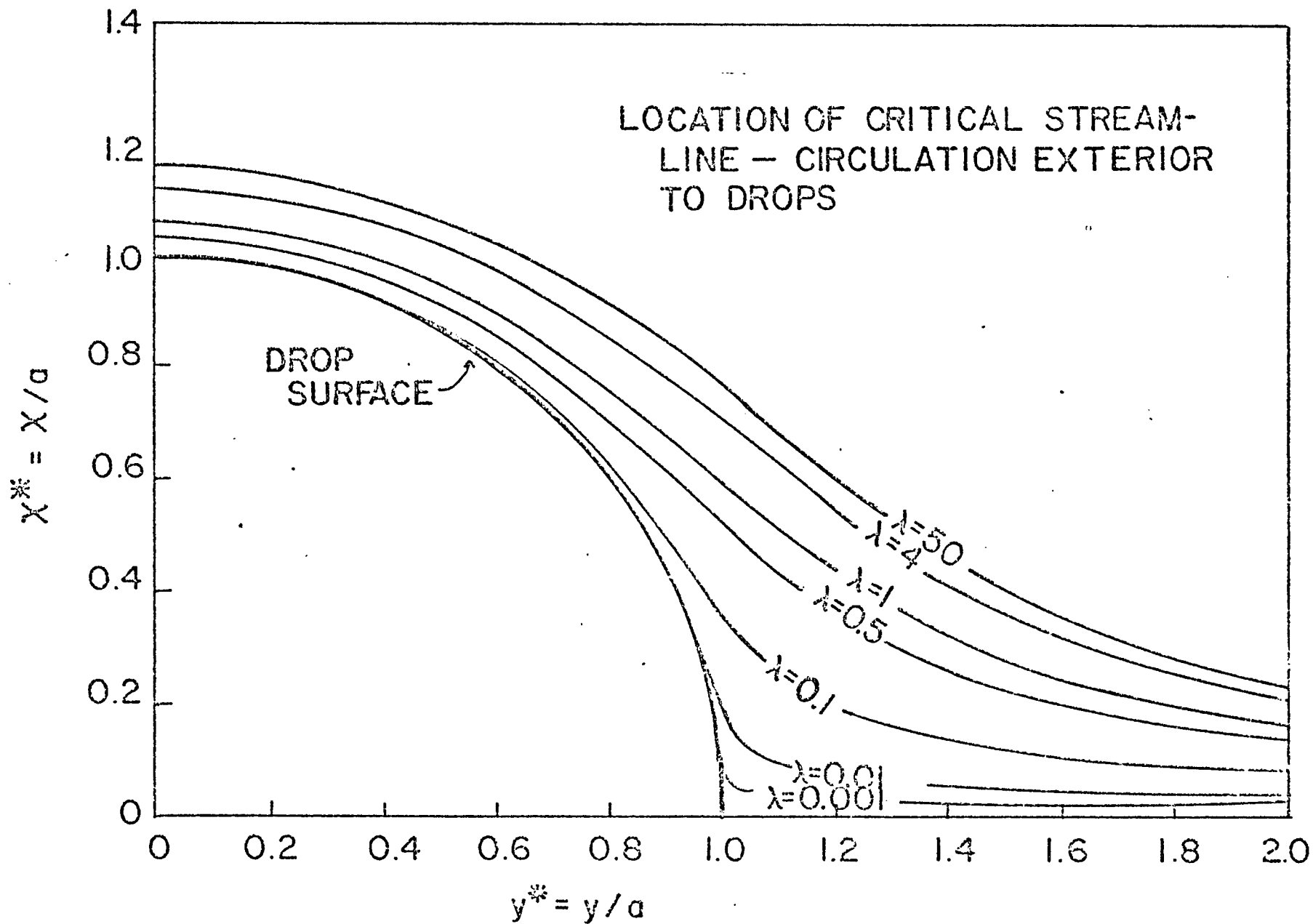


Figure 2.3-2. Positions of Drop Critical Streamlines for Various Values of λ

used to determine the value of λ from m and r_o , using an implicit numerical solution for λ devised by Phillips (9). For circulation at the drop's surface, Equation (2.3-2) can be reconstructed as follows to solve for λ

$$\lambda = \frac{m}{(m^2 - 1)} - 1 \quad (2.3-3)$$

Note that large errors can occur when calculating λ from values of m close to 1. Figure 2.3-1 also shows the insensitivity of λ when m is close to 1 for internal circulation. Notice also that as $\lambda \rightarrow \infty$ (corresponding to rigid body motion), the circulation number approaches one.

Tracer particles can also be used to find the paths of streamlines for particular values of r_o . An implicit numerical method formulated by Phillips (9) can then be used to calculate λ using r_o and two or more position data points. The measurement of the location of the critical streamline is a special case of these particular measurements. It is more sensitive to λ and thus a more accurate method for the determination of λ than other external streamlines. Figure 2.3-2 shows the limit of the critical streamline as $\lambda \rightarrow \infty$. This is the same critical streamline as that of a solid sphere.

For mainly experimental considerations, only the internal circulation time and critical streamline methods were attempted when studying drop circulations. External streamline and circulation time experiments require placement of tracer particles in the continuous phase near the drop. Achieving this is extremely difficult, and combining this with the fact that vertical fall velocities are different between a drop and tracer particles, ruled out these type of experiments. Only in the case of the critical streamline when a portion of the continuous phase can be

colored (such as by a dye, etc.) can external measurements be made. The critical streamline would be viewed experimentally as the boundary between two different colors, since no fluid within this streamline would escape its confines and mix with the rest of the fluid. For internal streamline and circulation time studies, however, tracer particles can be placed in the drop phase before the drops are injected into the continuous phase for experimentation. This has proven to be easier than the placement of tracer particles into the continuous phase for external streamline or circulation time experiments. For internal studies, the circulation time was found to be a more accurate method for the determination of λ than streamline positions. The period of circulation on the drop's interface is seemingly a good experiment, but λ is extremely sensitive to very slight changes of r_0 . To run an accurate experiment would require that the tracer particle be placed exactly on the drop's surface, which is very difficult.

In view of the preceding comments, only internal circulation time and critical streamline experiments were used. These experiments are designed to find $\lambda = N_\mu + 2(3N_\kappa + 2N_\epsilon)/5$, or

$$\lambda = \frac{\hat{\mu}}{\mu} + \frac{2}{5} \frac{(3\kappa + 2\epsilon)}{\mu a} \quad (2.3-4)$$

For a fluid system with known bulk phase viscosities, the interfacial viscosity combination $(3\kappa+2\epsilon)$ can be calculated after λ is determined for a given drop size. Note that:

1. As $N_\kappa, N_\epsilon \rightarrow 0$

$$\lambda = N_\mu \quad (2.3-5)$$

This would apply when the interfacial viscous effects are very small, or for very large drops ($a \rightarrow \infty$).

2. As $N_\kappa, N_\epsilon \rightarrow \infty$

$$\lambda = 3N_\kappa + 2N_\epsilon \quad (2.3-6)$$

This would apply when interfacial viscous effects dominate the bulk viscous effects, or when the drops are very small ($a \rightarrow 0$).

The individual values of κ and ϵ cannot be determined by these experiments alone since only the combination $(3\kappa + 2\epsilon)$ can be calculated. In combination with drop deformation results or some other technique, however, the individual values of κ and ϵ can be determined.

Unfortunately, the analysis used by Torza, et al. did not include mass transfer, or interfacial tension gradients. If we interpret N_κ to be $N_{\kappa + \mu}$ as we did in Section 2.2, the circulation and streamline results for λ can be used to include mass transfer effects. This interpretation has not been rigorously proven, but is assumed on the basis of the deformation analysis that included mass transfer and showed a correspondence between N_κ and N_{μ} . With this assumption, λ would be greater than N_μ for interfacial tension gradient effects, as well as κ or ϵ effects.

Rumscheidt and Mason (10) experimentally found that minute traces of surfactant impurities caused the rate of internal circulation to progressively decrease with the age of the drop, and often ceased completely. They also noticed that the rate of circulation could be increased by reducing contamination of the drop.

They calculated the force at the interface necessary to completely stop all internal circulation as

$$F = \frac{5}{2} \mu G a \quad (2.3-7)$$

Assuming that this force is generated by interfacial tension gradients caused by surfactants on the interface, they found that the necessary

gradient of interfacial tension to stop circulation is

$$F = \text{grad } \gamma = \frac{1}{k} \frac{\Delta c}{c} \quad (2.3-8)$$

where c is the concentration of surfactant on the interface and k is the interfacial compressibility. The Gibbs adsorption isotherm (6) relates $1/k$ to γ by

$$\frac{1}{k} = \frac{d\gamma}{d \ln c_s} \quad (2.3-9)$$

This is the same quantity as defined in Section 2.2. The quantity $\Delta c/c$ represents the amount of linear compression required to produce a change of concentration on the interface. Rumscheidt and Mason found that in many systems that have a large $(d\gamma/d \ln c_s)$, a very small linear compression is required to cause the requisite gradient of interfacial tension. As mentioned earlier, large values of $(d\gamma/d \ln c_s)$ are usually associated with systems having small concentrations of surfactant or impurity surfactants.

Their set of calculations clearly show how traces of surfactant impurities can have such an inhibitory effect on internal circulation. Such inhibition of circulation as this would show up as an increase in λ , since the limit as $\lambda \rightarrow \infty$ is the case for a rigid sphere. These comments are an indication that the assumption to interpret N_k as $N_k + \infty$ (so as to make the theory include interfacial tension gradient effects) may well be a valid assumption.

CHAPTER 3

EXPERIMENTAL STUDIES

3.1 Experimental Apparatus

All the experiments were conducted in a Couette apparatus, which consisted of two plexiglass, counter-rotating concentric cylinders. When set in motion, a shear field was established across the fluid in the gap between the cylinders. Figures 3.1-1 and 3.1-2 show a schematic diagram and picture of the experimental apparatus.

The radii of the inner and outer cylinders (R_i and R_o) are 11.75 cm and 13.34 cm, respectively. The gap between the cylinders is 1.59 cm, therefore, and the ratio of the gap width to inner radius is 0.135. With a small ratio of gap width to R_i , the curvature effects are small, and the generated shear field is very nearly a simple shear field. (Refer to Figure 2.1-1.) A stagnation point exists where $V_y = 0$, and a drop placed at this spot will remain stationary with respect to the x and y axes. The shear rate at the stagnation point is

$$G \Big|_{V_y=0} = \frac{2 \omega_o + \omega_i (R_i/R_o)^2}{1 - (R_i/R_o)^2} \quad (3.1-1)$$

where ω_i and ω_o are the angular velocities of the inner and outer cylinders.

Each cylinder was equipped with a variable motor drive (Electro-Craft Corporation, Model E 650-025) with additional reduction gears (486:1). The motor speeds were controlled by a separate control for each motor. A voltmeter measured the voltage across the tachometer to each motor, and the cylinder speeds were calibrated to the voltage readings. For this setup, an accurate working range for the shear rate was from 0.004

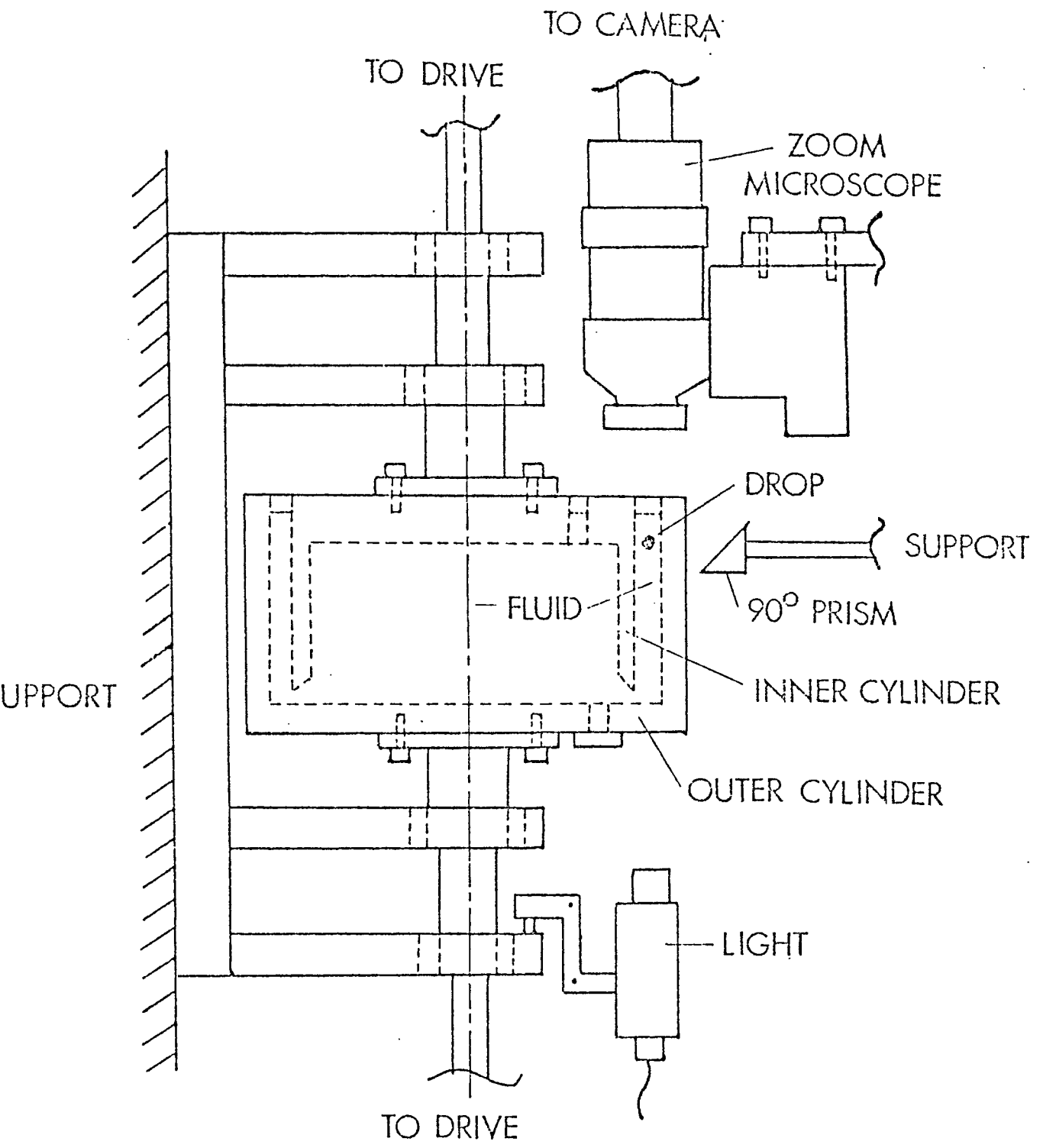


Figure 3.1-1. Schematic of the Experimental Apparatus

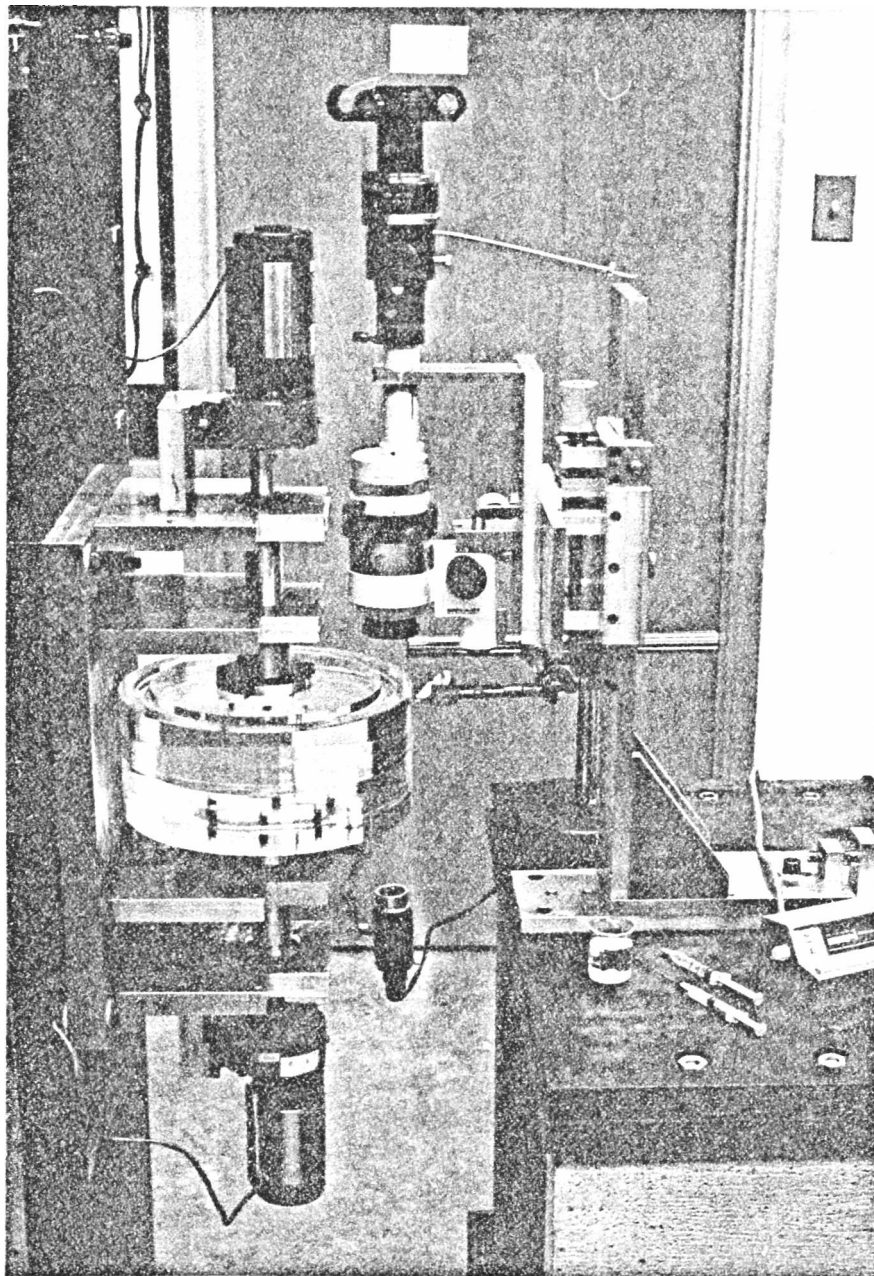


Figure 3.1-2. Photograph of the Experimental Apparatus

to 9.7 sec^{-1} .

The optical equipment consisted of a light source, a microscope, and two cameras. A high intensity lamp was mounted below the cylinders to provide lighting for viewing the experimental drops. The lamp had heat absorbing glass on it to avoid adding heat to the fluids. A Wild M7 Zoom Stereomicroscope provided magnification capability from 3 to 124x. Either of two cameras could be attached to the microscope to record the drop experiments on film. A Nikon Dark Box M-35S provided capability for 35 mm still photography, whereas a Beaulieu R16 provided 16 mm motion picture capability, with a range of filming speeds from 2 to 64 frames per second. A minimum working size for the drops was approximately $a=0.004 \text{ cm}$.

The microscope-camera system was mounted on a support that was capable of 3-directional movement, to facilitate adjustment to the desired position. The support for the microscope-camera was firmly attached to a concrete weighing table. This was necessary to avoid any slight motion that would blur the photography of the magnified drop. The microscope was normally placed in a position to view the drops from above the cylinders. Internal circulation experiments also required the drops to be viewed from the side. In this case, a prism was mounted by the Couette to project a side exposure of a drop to the microscope placed above the prism.

3.2 Experimental Procedures

To run the deformation experiments, a drop of one fluid was placed in the other fluid (the continuous phase) already in the annular region of the cylinders. Syringes were used to inject drops of various sizes.

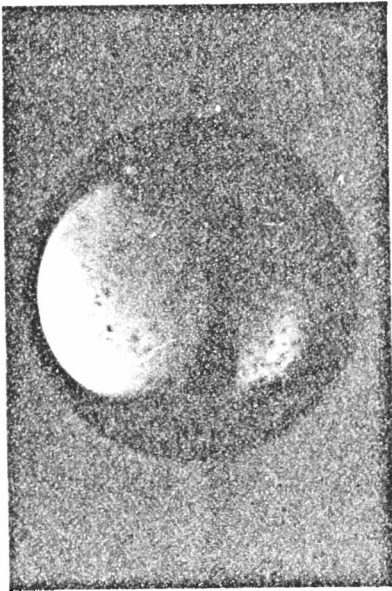
One of the drops was then selected and the experiment was begun.

Photography for deformation was taken with the still camera looking straight down at the drop. An undeformed drop was first photographed to obtain the undeformed radius "a". Then the cylinders were set in motion to obtain a desired deformation of the drop. A photograph was taken, and the speeds of the cylinders noted. This procedure was then repeated to obtain various deformations at different shear rates. Figure 3.2-1 shows a drop at various deformations. This entire procedure was repeated for various sized drops. For some of the drops, the time was noted each time a deformation was recorded. This was done to ascertain if there were any time dependent effects.

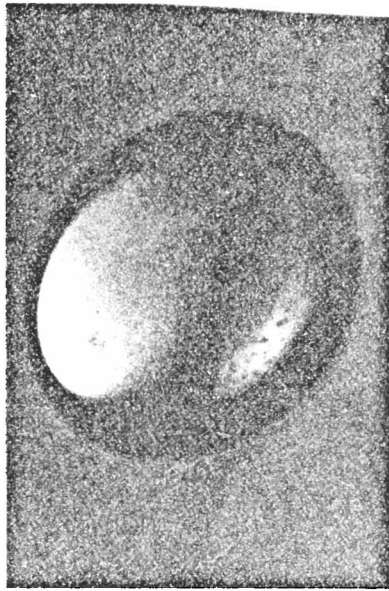
After completion of the experiment, photographs were also taken of a precision ball (Industrial Tectonics, Inc.) to calibrate the size of the photographs. Depending upon the magnification for each experiment, these sapphire balls had diameters of 1/32, 1/16, 3/32, and 5/32 inches, accurate to ± 0.0001 inches. In addition to this, photographs were taken of the edges of the two cylinders so that a perpendicular line to them could be constructed on the photographs. This was necessary when measuring the orientation angle (see Figure 2.1-1).

The experimental photographs were analyzed by using a slide projector to project their images onto a wall. The undeformed drop radius "a" and the deformation parameters L and B were determined from analyzing these projections, as well as the orientation angle α .

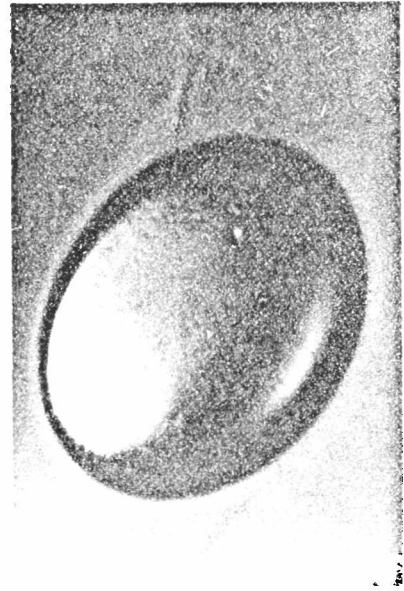
Internal circulation experiments required that tracer particles be used to time the periods of circulation around interior streamlines. Because the theoretical equations used in the analysis are valid only for streamlines in the drop's equatorial plane, the tracer particles



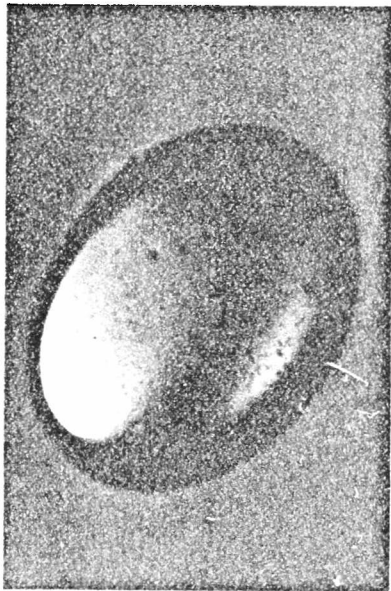
D = 0
 $\alpha = -$



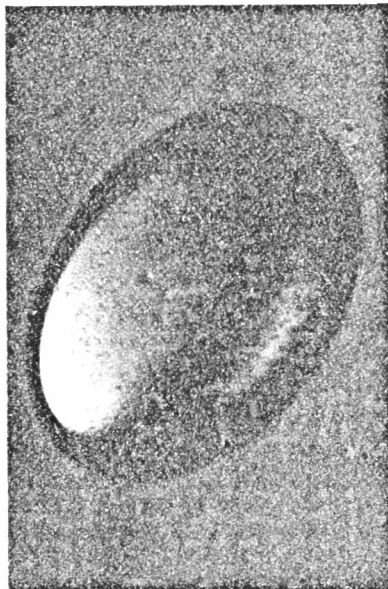
0.08
51°



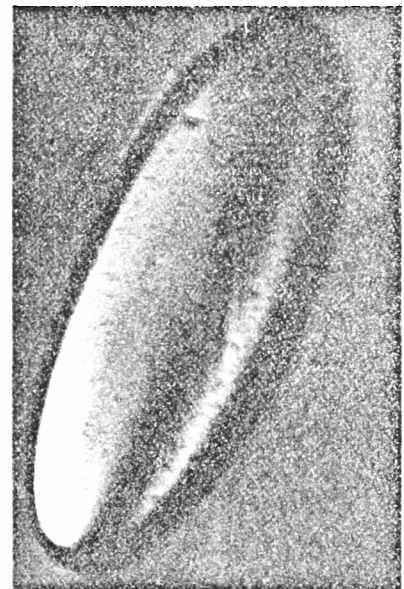
0.13
54°



D = 0.14
 $\alpha = 55^\circ$



0.19
58°



0.43
66°

Figure 3.2-1. Typical Drop Deformation Sequence (System B)

consequently must be in the equatorial plane, and stay there during the course of the experiment. The tracer particles, therefore, must have almost exactly the same density as the drop fluid for them to remain in the equatorial plane during the experiment. Solid tracer particles could not be found that had the same density as any of the fluids tested. A solution to this problem was found by dispersing a small amount of the continuous phase into the drop fluid before injection of the drops. These very fine droplets were of nearly the same density as the drop liquid because both test fluids were always of similar densities.

With a dispersion of the continuous phase in the drop fluid, the drop fluid was then injected into the Couette annular region with a syringe. A candidate drop was selected, but it had to be checked first to see if the tracer particle in it was in the drop's equatorial plane. To do this, the drop was viewed from the side by use of the prism (as already explained). The cylinders were activated, and if the tracer remained in the equatorial plane as it travelled around the drop, the microscope was returned to a position directly above the drop to begin the experiment. If not, the drop was rotated by agitating the continuous phase around it until the tracer was in the desired position.

The movie camera was selected to photograph the drop in this set of experiments. Shear was started by turning on the motors, and the tracer particle in the drop proceeded to circulate on its streamline. The drop was photographed at the camera's slowest speed, which calibrations found to be 2.18 frames per second. Filming was continued until the tracer made several revolutions, to make sure it remained on the same path and to see if the time of circulation changed. The cylinder speeds were also noted. If the drop had not yet fallen from view, a

new speed was selected (so long as the drop remained essentially undeformed), and the drop was photographed again at a new shear rate. The entire procedure was repeated for other drops to obtain readings of tracer circulation times at various radial positions. The sizes of the photographs were calibrated by filming precision balls.

For experimental analysis, the film was projected onto the wall. In a frame by frame analysis the position of the tracer was plotted as it circulated inside the drop. The radial position of the tracer at $\phi = 0$ (r_0) was found, and the period of circulation T was calculated by a count of the number of frames the tracer took to make one revolution. The radius of the drop was also calculated from the size-calibrated photograph.

The measured value of r_0 was not its actual value, however, due to refractive index differences between the drop and continuous phases. For internal circulation experiments, therefore, the refractive indices of the two fluids (n and \hat{n}) were determined. Using the values in a refraction calculation (see Phillips (9)) the actual value of r_0 was determined.

Critical streamline measurements were made on the first fluids tested (System A) because of a peculiarity of the fluids. The continuous phase was a mixture of glycerin and water (4% by vol.), which had a tendency to absorb slight amounts of water from the atmosphere because of the high glycerin content. When the cylinders were activated, the small amounts of water stayed segregated from the rest of the fluid until they eventually mixed completely into the continuous phase. While the small amounts of water were still unmixed, they could be seen as striations in the continuous phase because of a difference in refractive indices.

When a drop was placed into the fluid and the cylinders activated, the striations adjusted themselves to the critical streamline of the drop. The drop was then photographed (with either the still or movie camera). This procedure was repeated for different drops.

The photographs were projected on a wall for analysis, and the position of the critical streamline was traced. The drop radius "a" was also found from the size-calibrated photographs.

3.3 Materials and Physical Properties

Experimental and theoretical limitations placed severe restrictions on the choice of liquids used. A major problem encountered when running the experiments was vertical motion of the drops due to a density difference of the fluids. Keeping the drop in focus, and trying to keep it from falling from view made neutral buoyancy a desirable attribute of the pair of liquids studied. This could be achieved either by working with fluids of similar density and/or requiring that the continuous phase have a high viscosity. The theory also required that gravitational effects be small compared to viscous shear effects. This can be expressed by requiring

$$N_{gv} = \frac{(\rho - \hat{\rho}) ga}{\mu G} \ll 1 \quad (3.3-1)$$

where N_{gv} is called the gravitational-viscous number, which compares gravitational effects to shear viscous effects. In addition, the theory required that inertial effects be small compared to viscous effects (or having small Reynolds number). This latter criterion was always easy to satisfy in these particular experiments.

The desirability of the fluids having a small density difference

is offset by the requirements of making accurate interfacial tension measurements. Most techniques for measuring γ require that their density difference be known. The accuracy of measuring small differences of density goes down as the density difference becomes very small. Hence, there is a trade-off between having a sizable density difference for accurate γ measurements, and the desirability of a small density difference for the Couette experiments.

To make the densities of the fluids close to each other, a co-solvent was added in the proper proportions to change the density of the drop phase. The resulting drop fluid had to be insoluble in the continuous phase so that mass transfer of the bulk fluids would not occur. The liquid also had to be incompressible and of Newtonian behavior. The continuous phase had to be transparent so the drop could be viewed, and the drop phase needed to be transparent if internal circulation experiments were to be run.

The first liquid-liquid system chosen contained no added surfactant. This first fluid system, named System A, used a mixture of glycerin and water as the continuous phase and a mixture of mineral oil and tetrachloroethylene (TCE) as the drop phase.

The volume percentages of glycerin and water were 96% and 4%, respectively. This mixture had a fairly high viscosity, but also had Newtonian rheological characteristics. The high glycerin content of the continuous phase invited atmospheric water absorption. The mixture was well covered when not in use to avoid this from happening and changing the physical properties. A very small amount of water did absorb, however, which showed up as streaks or striations when the cylinders were activated. This was a very convenient condition, since the drop critical

streamlines could be studied.

A surfactant was added to the second system to obtain a very low interfacial tension. In addition to this, the experiments were conducted at a high concentration of surfactant where the curve of γ as a function of $\ln c_s$ flattens out. As explained in Section 2.2, this would be expected to yield a low value of N_{ω} , that is, achieve a condition where interfacial tension gradients would not occur. Hence, the κ and ϵ properties could be studied without interference.

An attempt was made to make this second system, System B, somewhat resemble the liquids encountered in micellar chemical flooding. A mixture of glycerin and water was chosen to resemble the aqueous phase, and a mixture of mineral oil and two co-solvents was elected to resemble the oil phase.

A higher percentage of water (25%) was chosen in this system than System A. The mixture would be more water-like and would also have a lower interfacial tension. Glycerin was still retained to keep the viscosity from becoming too small. Atmospheric water vapor was not absorbed in an amount necessary for striations to appear, as they did in System A.

A petroleum sulfonate was picked as the surfactant. It is produced by Witco Chemical Company under the designation Petronate TRS 10-80. Having an average molecular weight of 405, it is described as being composed of 80% petroleum sulfonate, 11.3% mineral oil, 8.0% water and 0.7% inorganic salt. Besides the surfactant, sodium chloride was added to lower the interfacial tension. The surfactant and salt were each added to the glycerin-water solution in the amounts of 0.01 grams per gram of glycerin-water.

For System B, 1,1,2,2-tetrabromoethene (TBE) was used as a co-solvent because it has a much higher density than TCE. The TBE would not dissolve completely in the mineral-oil, however, so a little TCE was added with it to make the TBE completely dissolve into the solution.

Except for the surfactant and salt, the two phases were insoluble in each other. To distribute the surfactant and salt into the drop phase, the mineral oil-TBE-TCE was equilibrated with the continuous phase prior to experimentation. To do this, a small volume of drop phase was shaken together with a larger volume of continuous phase, in the ratio of about one to seven. The fluids were left until they completely separated, roughly one to four days, and then the equilibrated drop phase was ready for experimental use.

The physical properties of the drop and continuous phases of both Systems A and B are shown in Table 3.3-1. All drop deformation, internal circulation and critical streamline experiments were conducted in a laboratory maintained at $25.0^{\circ}\text{C} \pm 0.5^{\circ}\text{C}$, as were all physical property measurements. Viscosity measurement for all fluids were determined from Cannon-Fenske viscometers. The densities of System A fluids were found by using pycnometers, whereas System B densities were determined by a Westphal balance. The refractive indices of all fluids were found by use of an Abbe refractometer.

The interfacial tensions were measured by two different methods. The pendant drop method, suitable for the measurement of high interfacial tension, was used for System A, and the spinning drop method, designed for very low interfacial tensions, was used for System B. The Spinning Drop Interfacial Tensiometer (Model 300) was manufactured by the University of Texas. The pendant drops were magnified and photo-

Table 3.3-1

Physical Properties of Materials

<u>System</u>	<u>μ (poise)</u>	<u>$\hat{\mu}$ (poise)</u>	<u>ρ (g/cm³)</u>	<u>$\hat{\rho}$ (g/cm³)</u>	<u>γ (dyne/cm)</u>	<u>n</u>	<u>\hat{n}</u>
A	4.165	0.01844	1.2474	1.2874	22.8	1.466	1.476
B	0.4824	0.2651	1.2128	1.1725	0.079	1.4432	1.4945

System A

Continuous Phase = Glycerin (96 vol. %) and Water (4%)

Drop Phase = Mineral Oil (45 vol. %) and Tetrachloroethylene (55%)

System B

Continuous Phase = Glycerin (75 vol. %) and Water (25%) + 0.01 $\frac{\text{g salt}}{\text{g Glycerin-Water}}$ + 0.01 $\frac{\text{g Witco 10-80}}{\text{g Glycerin-Water}}$

Drop Phase = Mineral Oil (82 vol. %) and 1,1,2,2-Tetrabromoethane (14.4%) and Tetrachloroethylene (3.6%)

graphed with the same microscope-camera system used in the Couette experiments, only in this case the apparatus was mounted horizontally to view the drop from its side. The film was projected on the wall, and the shape factors were then determined.

Both measurements required some time for the interfacial tension to reach its equilibrium value. The pendant drop interfacial tensions came to equilibrium in about five to ten minutes. The interfacial tensions measured in the spinning drop apparatus dropped rapidly with time, and then approached equilibrium after anywhere from five to forty minutes. In most tests, however, equilibrium values were attained after approximately ten to fifteen minutes. Because the interfacial tension of fresh drops required time to reach equilibrium, data for the drop deformation experiments was checked to see if the results changed with time. It should be recalled that the interfacial tension value is necessary in deformation analyses, but not in circulation or critical streamline analyses. A change of results with time would presumably mean that the interfacial tension had not yet reached a steady value. No direct correspondence could be made to estimate the time necessary for equilibrium to be reached in the Couette from times of the pendant and spinning drop tests, since drop size was smaller in the Couette.

CHAPTER 4

RESULTS AND DISCUSSIONS4.1 General Data Analysis

The two liquid systems already described were studied to find the magnitudes of the interfacial dilational viscosity, the interfacial shear viscosity, and interfacial tension gradients. A simple shear field was generated in the continuous phase of each system by the Couette apparatus, and the behavior of the drop in such a flow field was studied.

The deformation and orientation angle were analyzed in deformation tests done on both systems, as was the period of internal circulation of a tracer particle on internal streamlines. The critical streamline of System A drops was also studied. The shear rate for all experiments was calculated from the angular velocities of the cylinders, using Equation (3.1-1). In addition, the parameter N_{μ} was calculated from the ratio of the drop phase viscosity to the continuous phase viscosity (Equation (2.1-2)).

The raw data of the deformation experiments were the undeformed drop radius, the length and width of the deformed drop, its orientation angle, and the shear rate. Combined with the bulk physical properties, the deformation and the dimensionless shear rate were calculated from Equations (2.1-4) and (2.1-3), respectively. Consequently, D/N_G was found. The quantity λR was calculated from Equation (2.2-28). The D/N_G and λR data for each drop were averaged to obtain more reliable values for each particular drop. Then γ_{eff}/γ was calculated from Equation (2.2-34) with the average value for D/N_G . For all subsequent analyses (except as otherwise noted), the data points used were the average values for each drop.

The values for N_{gv} were calculated from Equation (3.3-1). In Appendix I the data for "a", G , N_{gv} , D , N_G , D/N_G , D/N_G (avg), γ_{eff}/γ , α , λR , and $\lambda R_{(avg)}$ are given. Some of the drops also show the D/N_G data as a function of time.

The raw data for internal circulation experiments were the drop radius, the shear rate, the period of circulation, and the dimensionless radial position of the tracer particle's path at $\phi = 0$. The circulation number m was then calculated using Equation (2.3-1). The data for "a", G , T , r_o , and m are given in Appendix I.

The critical streamline data were the positions of the critical streamline. The values for "a", G , x^* , and y^* for System A are in Appendix I, where x^* and y^* are the dimensionless x and y coordinates of the critical streamline's position.

Some attention must be made to the experimental errors encountered in these experiments. A summary is made here of the standard deviations calculated for measured data and finished data in Appendix II.

The variables D/N_G and λR had fairly large errors due to the nature of the equations from which they are derived. D is calculated from $(L-B)/(L+B)$, so a small error in L or B will cause a fairly sizeable error in D . The major error in calculating N_G is from γ , which in turn suffers from errors when the density difference between the two test liquids becomes small. The standard deviation found for D/N_G is about 7.1%.

The values for λR are extremely sensitive to α . The α for System A were only found to an accuracy of about 4 degrees, whereas α for System B were found to within 2 degrees of accuracy. This is because a better technique for determining the perpendicular line to the

Couette cylinders was discovered after System A experiments were completed. Regardless, the standard deviation of λR for System A is about 43% and for System B is about 20%.

Standard deviations for internal circulation and critical streamline tests were somewhat smaller. The standard deviations for key quantities are 5.2% for m , 4.3% for r_o , and 3.6% for both x^* and y^* . The standard deviation for "a" is 0.6%.

4.2 System A Results

System A was intended to be a "pure" system, or one with no added surfactant in it. This would serve as a basis to compare with the results of a low interfacial tension, surfactant system (System B). As already mentioned, the continuous phase consisted of glycerin and water, and the drop was a mixture of mineral oil and tetrachloroethylene.

Drop deformation experiments were performed, and data for various sized drops were obtained. The following theoretical constraints were all satisfied: 1) steady, incompressible flow, 2) Newtonian fluids, 3) small Reynolds number, and 4) small N_{Gv} . The individual data points of D/N_G as a function of time for two drops are shown in Figure 4.2-1. No time effects are apparent, so the interfacial tension was presumably at equilibrium. In addition, the deformation parameter D was always less than 0.18.

The data was analyzed by the equations that predict the deformations and orientation angles of drops over a full range of N_G values. These equations, (2.2-13) and (2.2-19), enable κ and ϵ to be calculated from D , N_G , and α data. When N_G is small, Equation (2.2-13) collapses to Equation (2.2-21). Consequently, the analysis of the data becomes

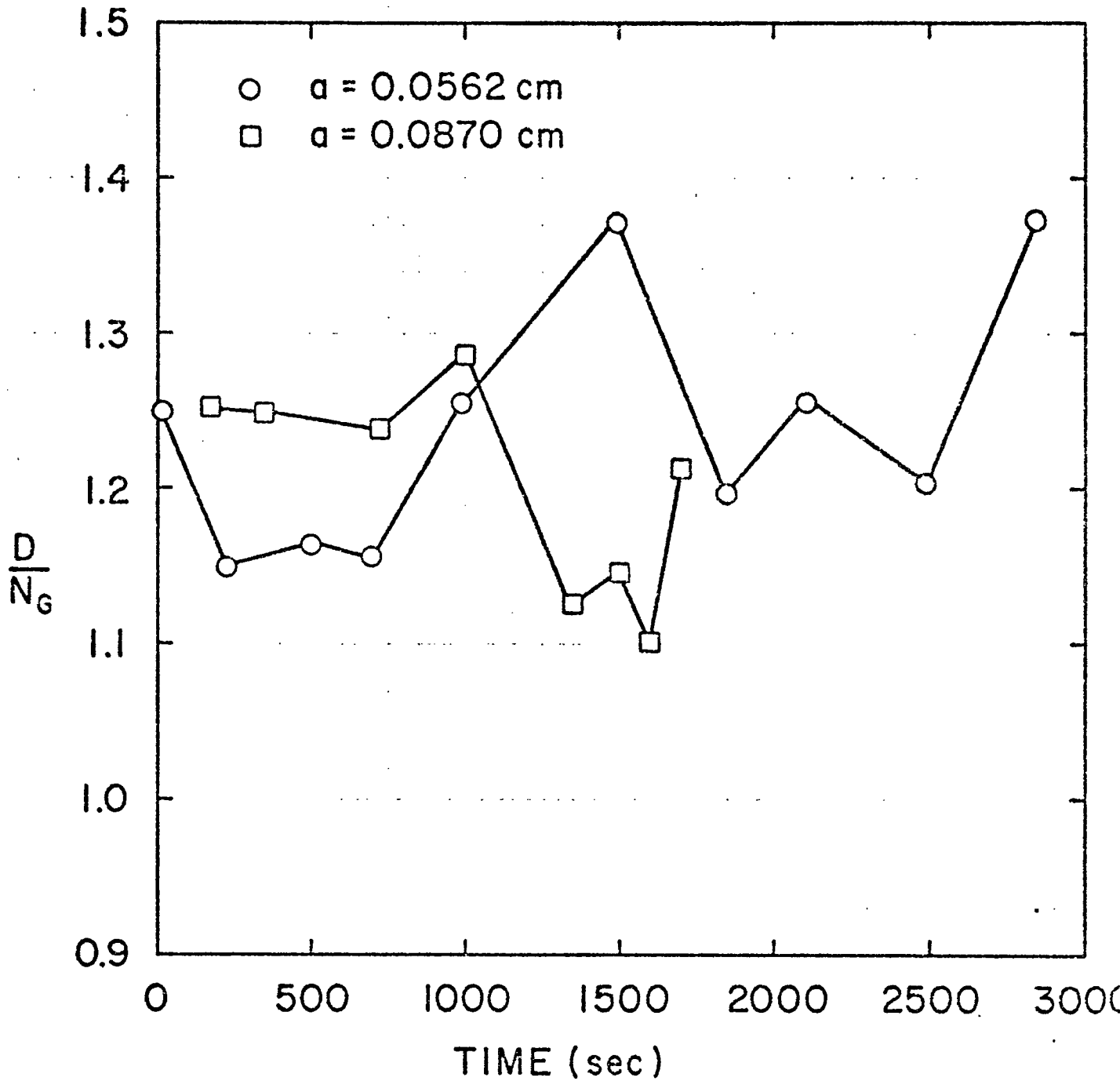


Figure 4.2-1. Time Dependence of Deformation: System A

easier because both D/N_G and λR are only functions of κ , ϵ , and "a", and are independent of N_G . Since the values of N_G data were always less than 0.15 for System A, the use of Equation (2.2-21) was justified.

The average values of D/N_G and λR for the drops are plotted in Figures 4.2-2 and 4.2-3 against the drop radius. These data were optimized in Equations (2.2-21) and (2.2-19) with respect to κ and ϵ in a nonlinear least squares computer routine (1). The best fit was obtained for $\kappa = 3.33$ s. poise (surface poise) and $\epsilon = 0.81$ s. poise. (The units of "surface poise" are cm-poise, or g-sec^{-1} .) The D/N_G and λR equations were plotted using these values for κ and ϵ , as well as when κ and ϵ equal zero, corresponding to Taylor's results. A comparison of the curves shows the existence of dynamic interfacial forces in System A.

The sensitivity of the equations to the experimental data needs to be considered. The equation for D/N_G is best for looking at the relative value of the ratio of κ to ϵ , whereas the λR equation is more suited for considering the magnitude of the combined effects. With this in mind, curves for D/N_G and λR were graphed for various κ/ϵ and $(\kappa+\epsilon)$, respectively, in Figures 4.2-4 and 4.2-5.

The value of $\kappa = 3.33$ s. poise (from the least squares minimization) was held constant when κ/ϵ was varied in the equation for D/N_G . A comparison of the experimental data of Figure 4.2-2 with the curves of Figure 4.2-4 shows that the ratio of κ/ϵ is somewhere in the range of 3 to 30.

For the λR curves at various $(\kappa+\epsilon)$, the ratio of $\kappa/\epsilon = 4.11$ ($3.33/0.81$) was held constant. With respect to Figure 4.2-5, the experimental data of Figure 4.2-3 would lie in the neighborhood of $(\kappa+\epsilon)$ equals 2 to 7 s. poise.

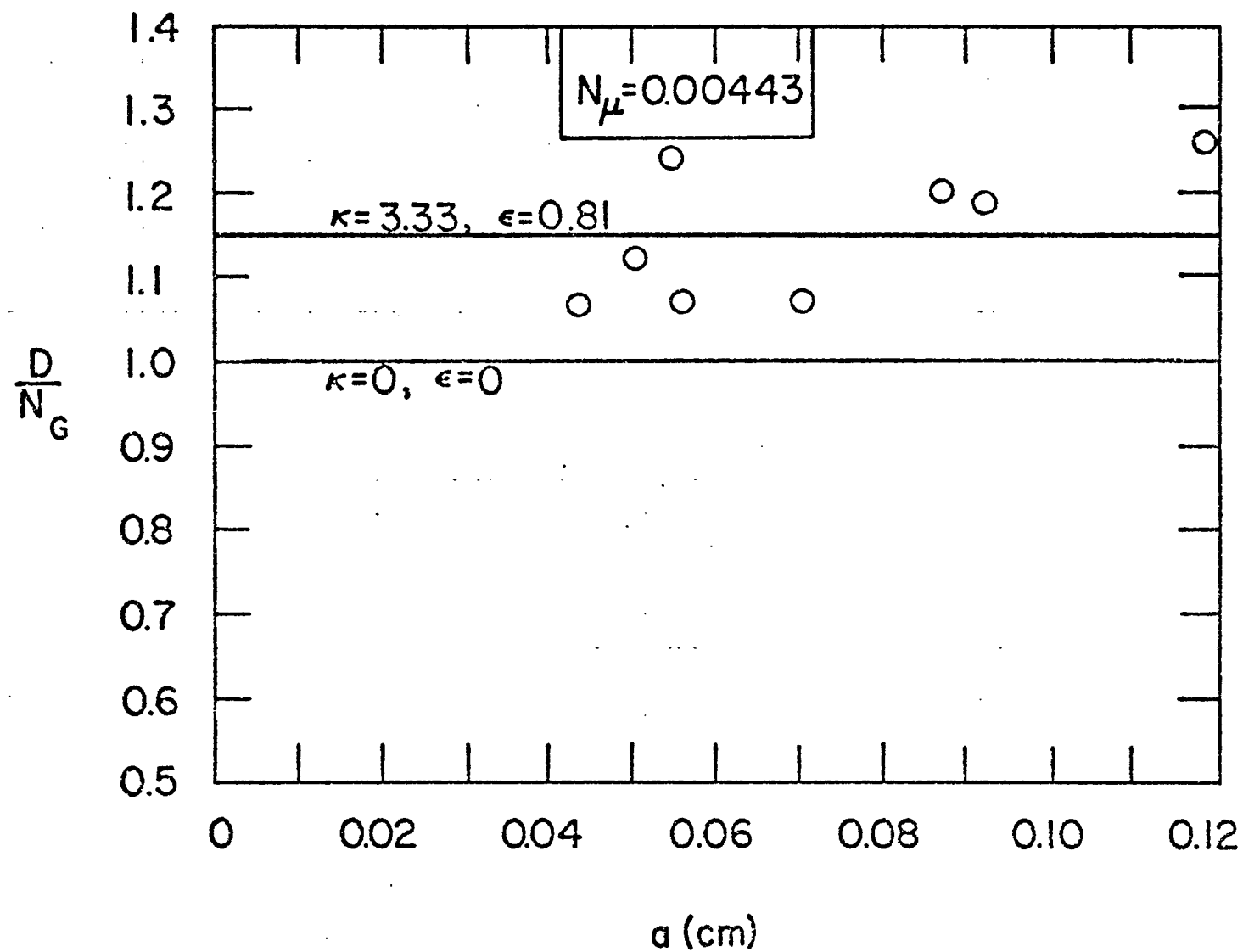


Figure 4.2-2. Deformation Data (D/N_G) and Fitted Curve: System A

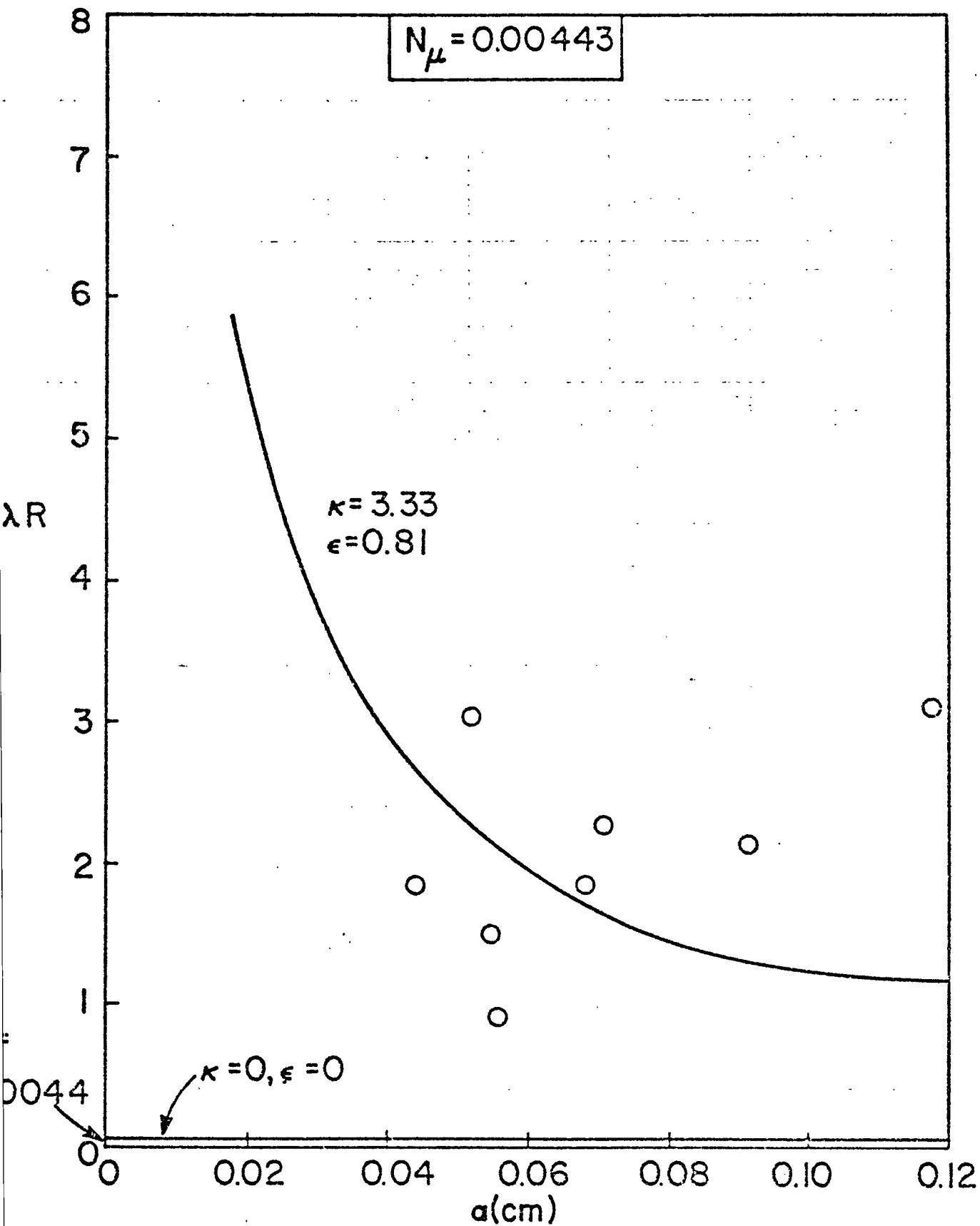


Figure 4.2-3. Deformation Data (λR) and Fitted Curve: System A

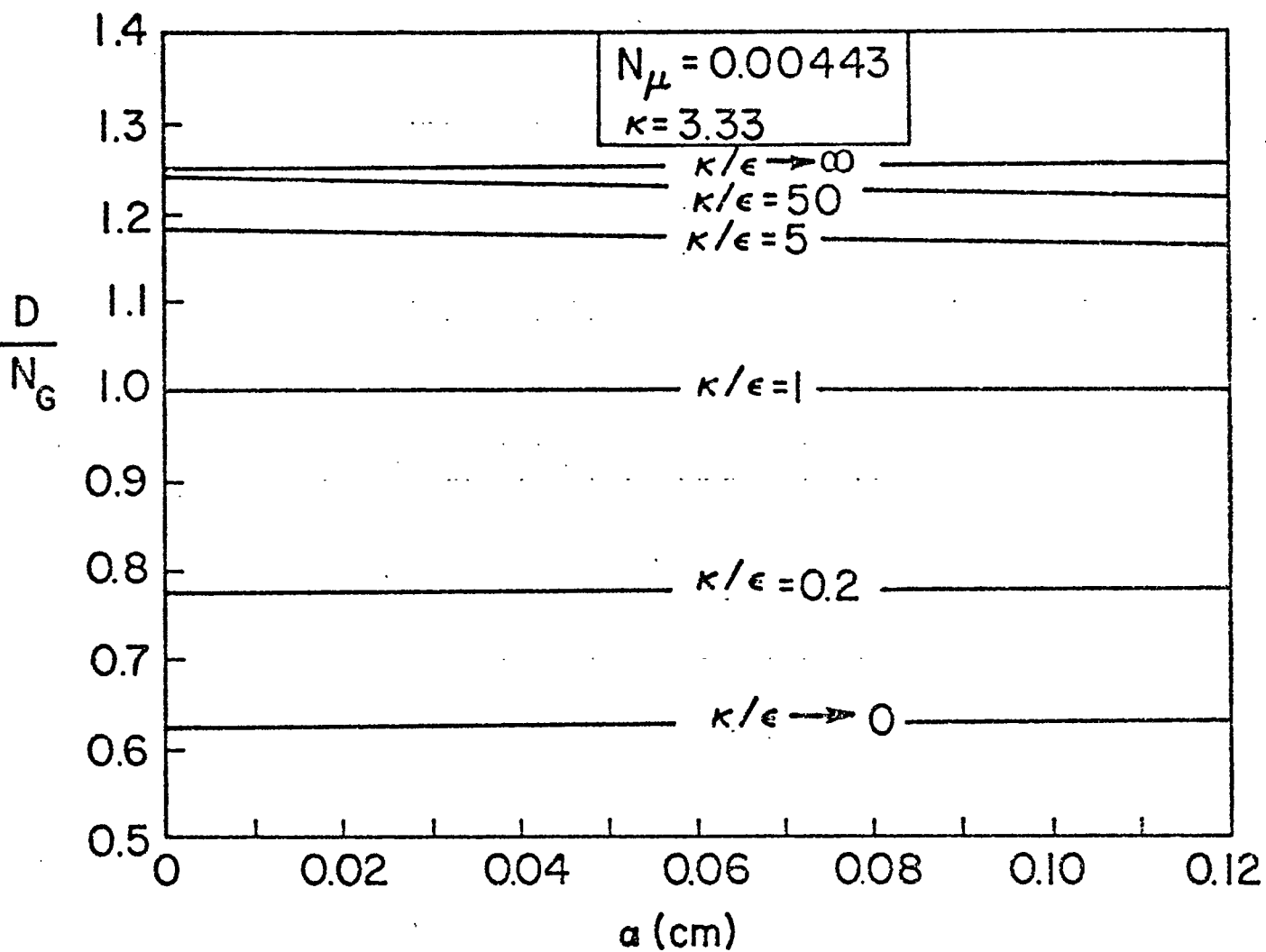


Figure 4.2-4. Deformations (D/N_G) for Various Values of κ/ϵ : System A

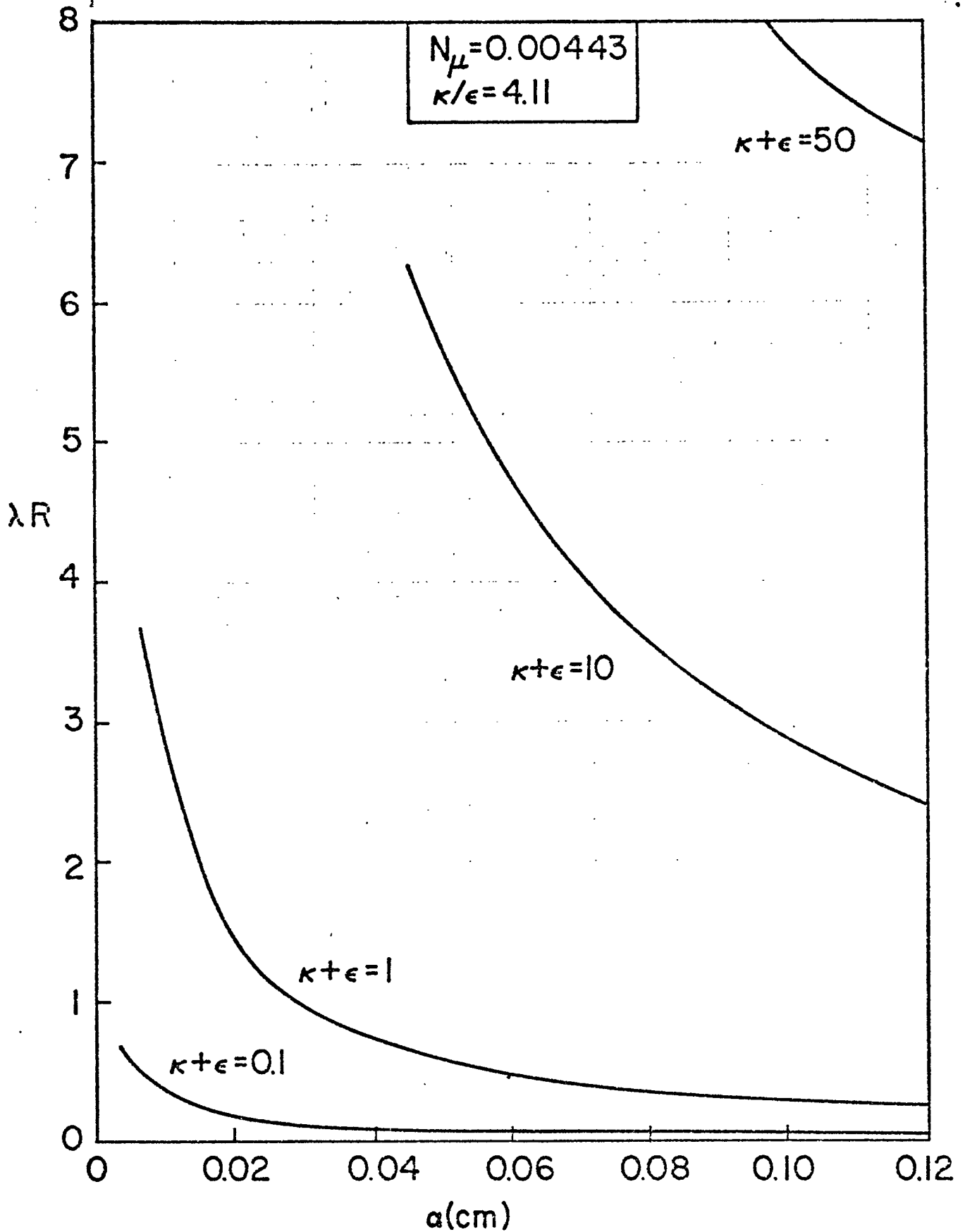


Figure 4.2-5. Values of λR , from Drop Deformations, for Various Values of $\kappa + \epsilon$: System A

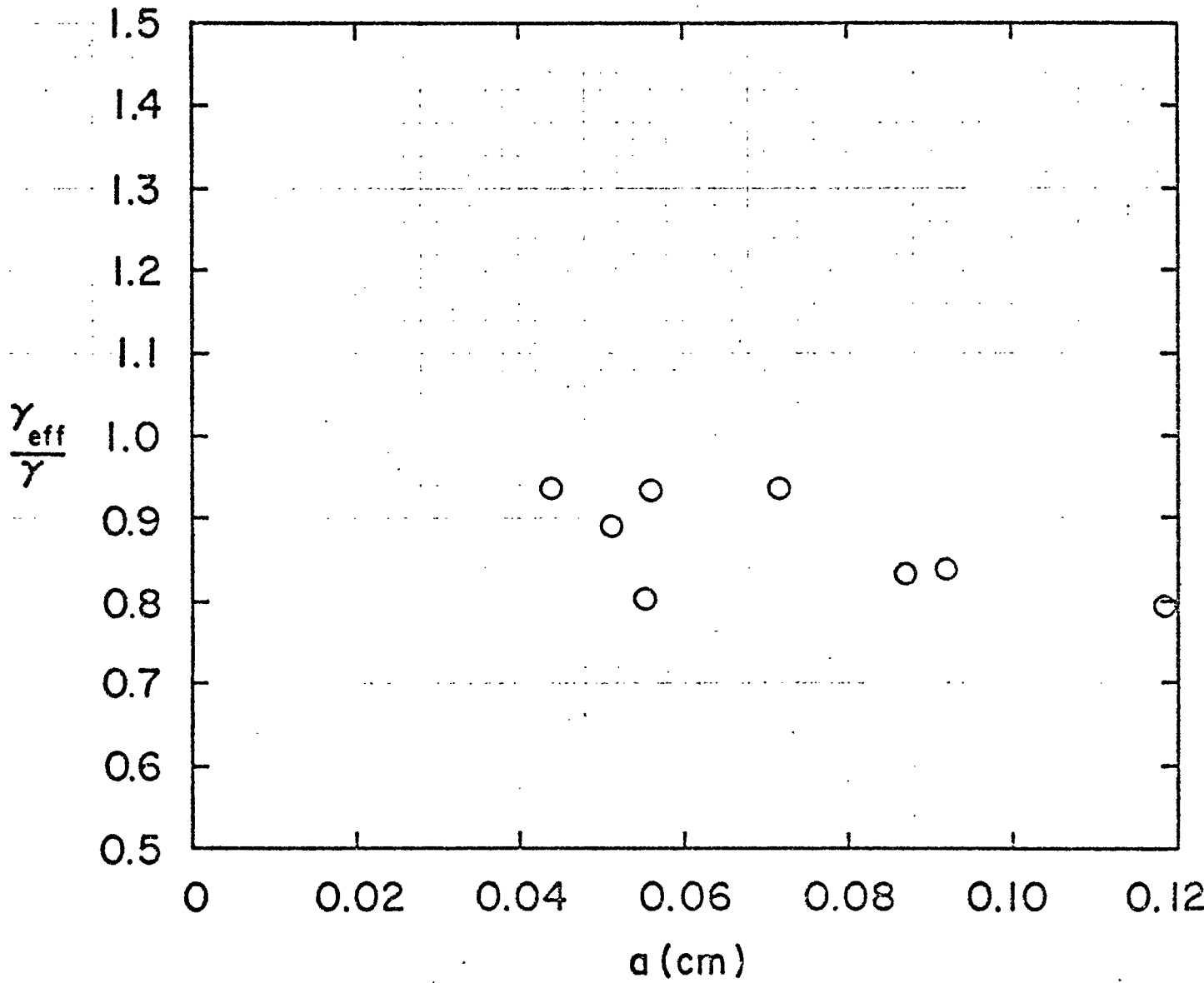


Figure 4.2-6. Data of γ_{eff}/γ from Drop Deformations: System A

Experimental errors can account for the scatter of the data around the curves for large κ and moderate ϵ values, but could not cause the data to have values so distant from the κ and $\epsilon = 0$ curves.

Unfortunately, the theory does not include interfacial tension gradient effects. But Equation (2.2-12) shows that κ effects can be caused by either the interfacial dilational viscosity or by gradients of γ (showing up as N_{σ}). The interfacial tension gradients could possibly be explained by trace impurities in the fluids which act as surfactants and collect on the interface. The discussion in Section 2.2 demonstrated that N_{σ} becomes very large for small surfactant concentrations because $(d\gamma/d \ln c_s)$ tends to be very large at these small concentrations. Consequently, no conclusion can be made concerning which effect, κ or $\text{grad } \gamma$, is mainly responsible for the observed behavior.

The deformation data does show evidence that a strong κ -type effect (either κ or $\text{grad } \gamma$) is present in System A. It also suggests that a smaller effect from the interfacial shear viscosity is present.

The net effect on the deformation is represented by $\gamma_{\text{eff}}/\gamma$ in Figure 4.2-6. The values for $\gamma_{\text{eff}}/\gamma$ range between 0.8 and 0.95. This clearly illustrates the presence of dynamic interfacial forces in System A.

Internal circulation and critical streamline experiments were also performed for System A. All of the theoretical criteria were satisfied in these tests, including the one that the drops must be nearly spherical.

The data for m as a function of r_0 were plotted in Figure 4.2-7 for internal circulation, and the position of the critical streamline was plotted from x^* and y^* data in Figure 4.2-8. A value of $\lambda = 20$ was

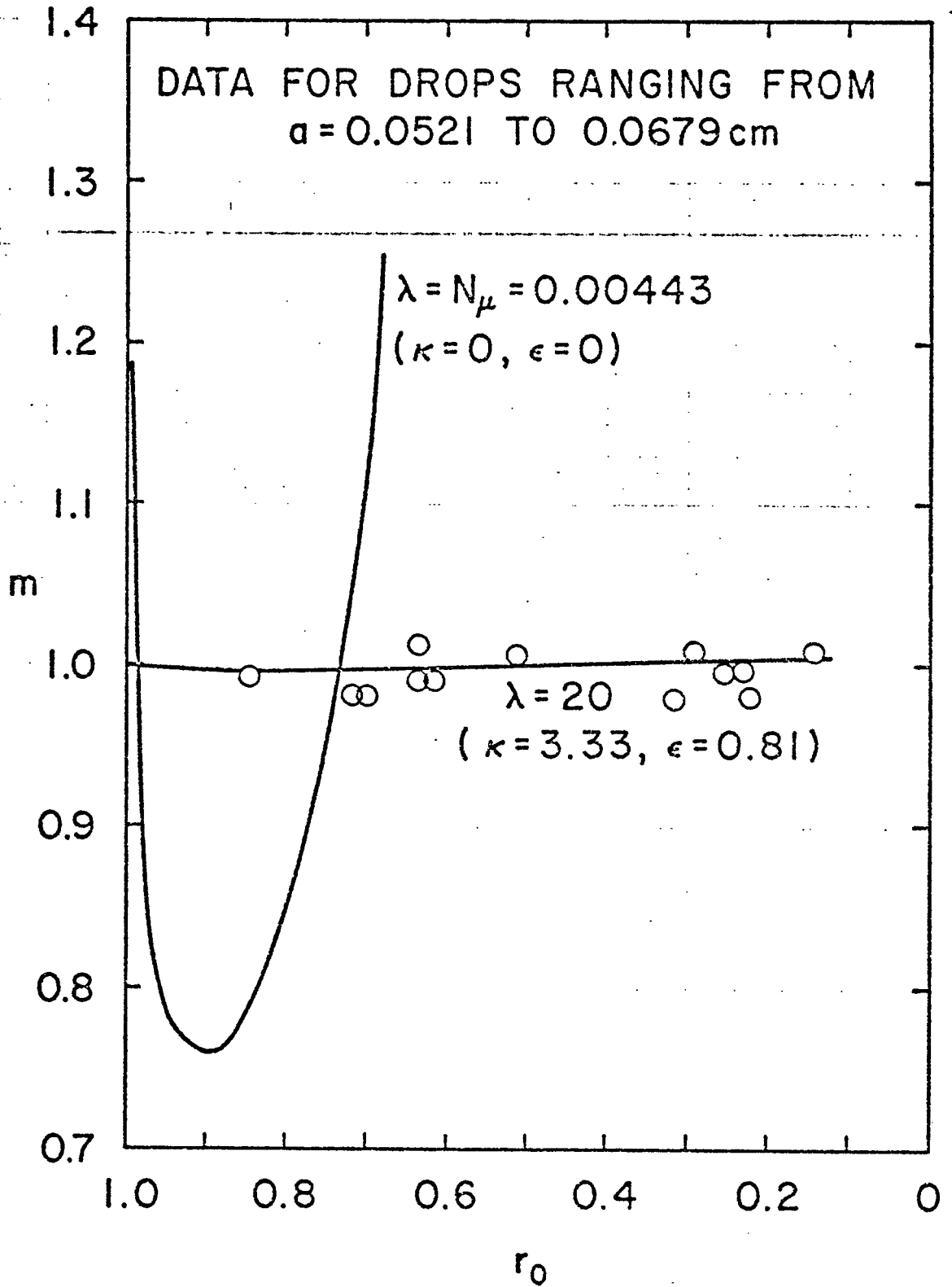


Figure 4.2-7. Experimental Internal Circulation Times and Fitted Curve:
 System A

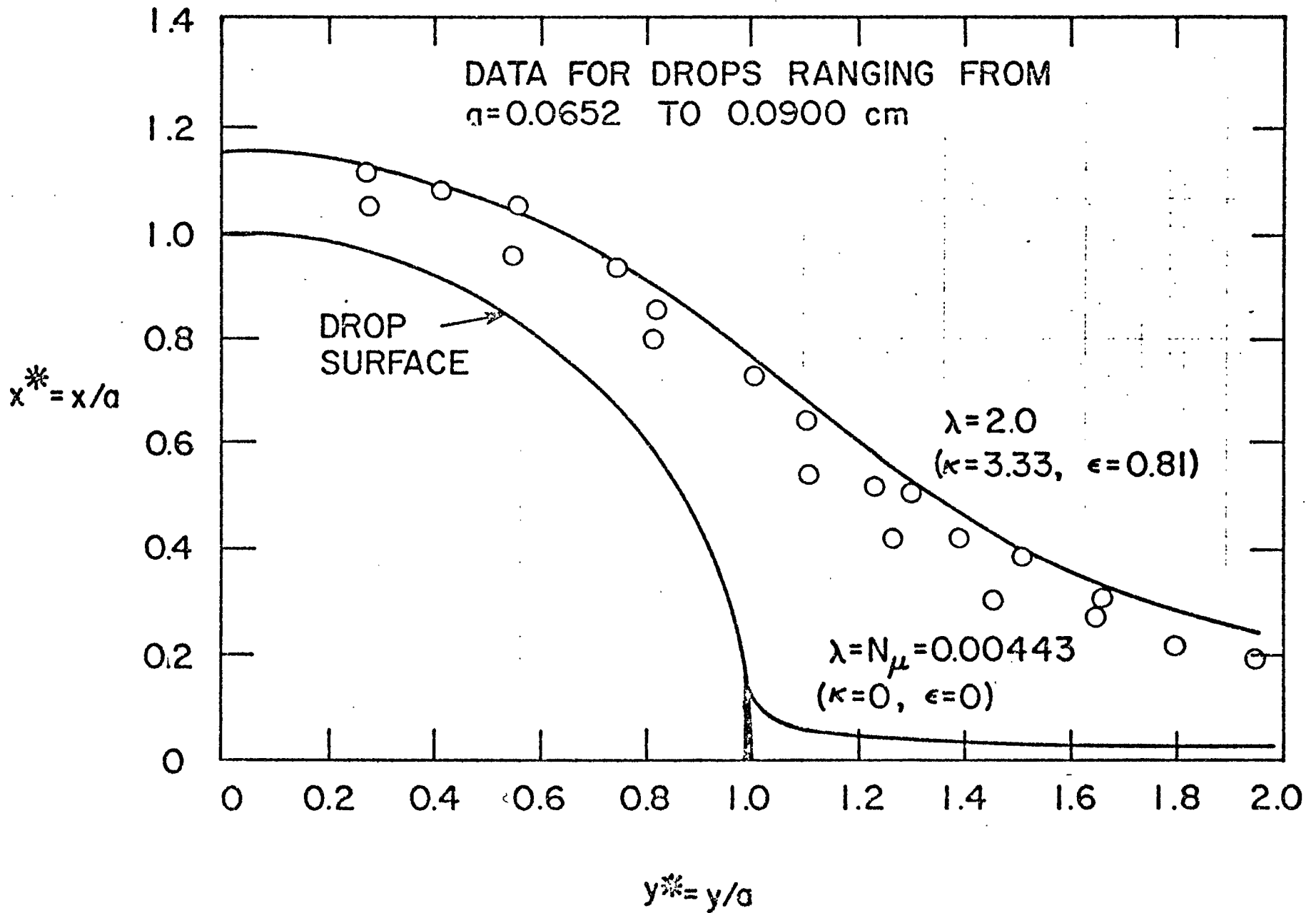


Figure 4.2-8. Experimental Critical Streamline Position and Fitted Curve: System A

plugged into the equations derived by Torza, Henry, Cox, and Mason, so that the curves for internal circulation times and the critical streamline could be plotted in the aforementioned figures. (Computations were achieved by using Phillips' computer routines.) Curves for $\lambda = N_\mu$ were also plotted. The $\lambda = N_\mu$ value corresponds to κ and $\epsilon = 0$, and the value of $\lambda = 20$ was computed (refer to Equation(2.2-15)) using the values of $\kappa = 3.33$ s. poise and $\epsilon = 0.81$ s. poise (from the minimization of the deformation data), and a value of about 0.06 cm for "a".

Although Figures 2.3-1 and 2.3-2 show that the accuracy of determining λ lessens as it becomes large, the data nevertheless show strong λ effects, and that λ is nowhere close to being equal to N_μ . The data, in fact, are very close to $\lambda \rightarrow \infty$, or rigid body motion. Experimental errors could not account for so great a difference between the data in the neighborhood of $\lambda = 20$, and the curve for $\lambda = N_\mu = 0.00443$.

Such a high value for λ is a result from either large κ or ϵ values. The κ effect, however, may not have been caused by the interfacial dilatational viscosity, but by interfacial tension gradients, as discussed in Section 2.3. These would show up in the N_σ portion of $N_{\kappa+\sigma}$. Impurities in the bulk liquids that act as surfactants and collect at the drop interface could result in large values of $(d\gamma/d \ln c_s)$. Hence, N_σ would be large, and the impurities could be responsible for making the drops appear to have rigid body motion, as suggested by Rumscheidt and Mason.

These researchers derived

$$F = \frac{5}{2} \mu G a \quad (2.3-7)$$

to represent the interfacial tension gradient necessary to completely

stop internal circulation. The gradient force was related to the linear compression on the surface by

$$F = \text{grad } \gamma = \frac{1}{k} \frac{\Delta c}{c} \quad (2.3-8)$$

Rumscheidt and Mason suggested that a reasonable value for k for a condensed monolayer is 10^{-2} cm/dyne.

For internal circulation in System A, typical values for Ga were about $0.025 \text{ cm-sec}^{-1}$. The force calculated from Equation (2.3-7) becomes (for $\mu = 4.165 \text{ poise}$) $F = 0.26 \text{ dyne-cm}^{-1}$, which is small. Combining this with Equation (2.3-8) and $k=10^{-2} \text{ cm-dyne}^{-1}$ yields $\Delta c/c=0.0026$. As explained by Rumscheidt, et al., this means that as an element of interface rotates over one quadrant of the drop's interface, a linear compression of only 0.26% followed by the same expansion over the next quadrant is sufficient to prevent internal circulation. They say "It is not difficult to imagine how the rotation of the sphere could accommodate itself to produce the necessary changes in surface concentration." These calculations show that trace impurities have the potential to cause large inhibitory effects by the creation of interfacial tension gradients. These considerations, however, still cannot rule out the possibility of interfacial dilational viscosity effects as the cause of the κ -type effects.

The possibility exists that impurity surfactants on the surface of the drop may also change the interfacial shear viscosity of the drop from its ϵ value prior to attachment of the molecules to the surface. This result would be caused by intrinsically changing the nature of the interface. This effect would be in addition to the effect the impurities could have on the interface by causing interfacial tension gradients.

A review of the results from drop deformation, internal circulation and critical streamline experiments show that they agree very well with each other. The drops which were tested, reacted to strong κ -type effects and lesser ε effects. Though exact values cannot be given, the effect from either the interfacial viscosity or interfacial tension gradients is somewhere around 3.33 s. poise, and the interfacial shear viscosity has a value of roughly 0.81 s. poise. These effects were possibly caused by trace impurities that acted as surfactants on the drop surface.

4.3 System B Results

A petroleum sulfonate surfactant was added to System B to find the interfacial dynamic effects of a low interfacial tension system. The concentration of surfactant was at the point where the curve of γ as a function of $\ln c_s$ flattens out (see Figure 4.3-1). With a small value of $(d\gamma/d \ln c_s)$, the quantity N_{2g} would also be expected to be small, and the interfacial viscosities could be studied more easily.

The fluids of System B somewhat resembled the liquids encountered in micellar chemical flooding. The drop phase (akin to an aqueous phase) consisted of glycerin and water. Mineral oil and two co-solvents (1,1,2,2-tetrabromoethane and tetrachloroethylene) served as the continuous phase, or "oil phase." As described earlier, 0.01 weight fraction of surfactant and the same weight fraction of salt were added to the glycerin-water, and the resulting fluid was equilibrated with the mineral oil-TBE-TCE liquid to prepare the drop phase for experimentation.

Drop deformation experiments were performed for System B. These

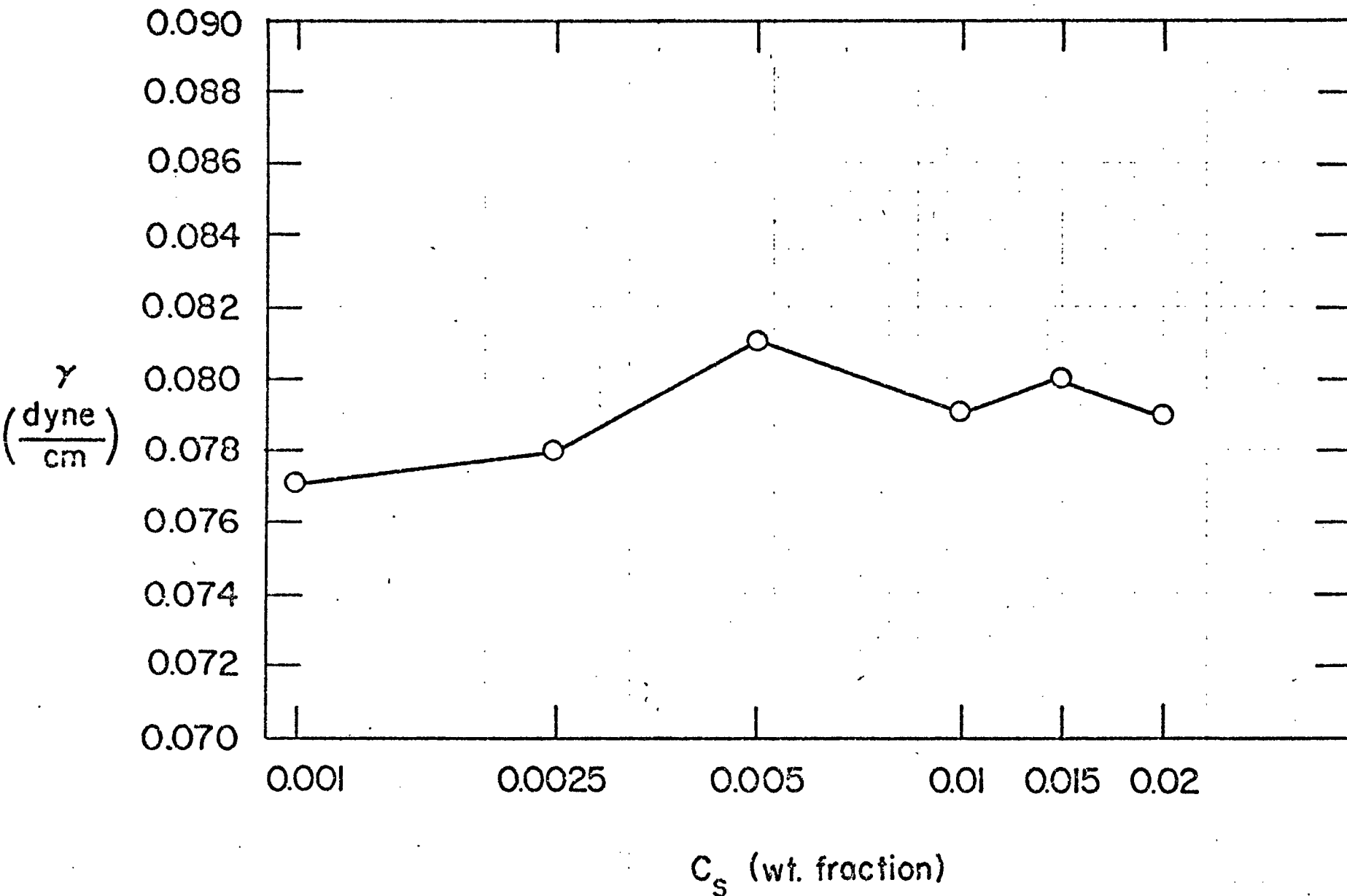


Figure 4.3-1. Dependence of Interfacial Tension on Surfactant Concentration: System B

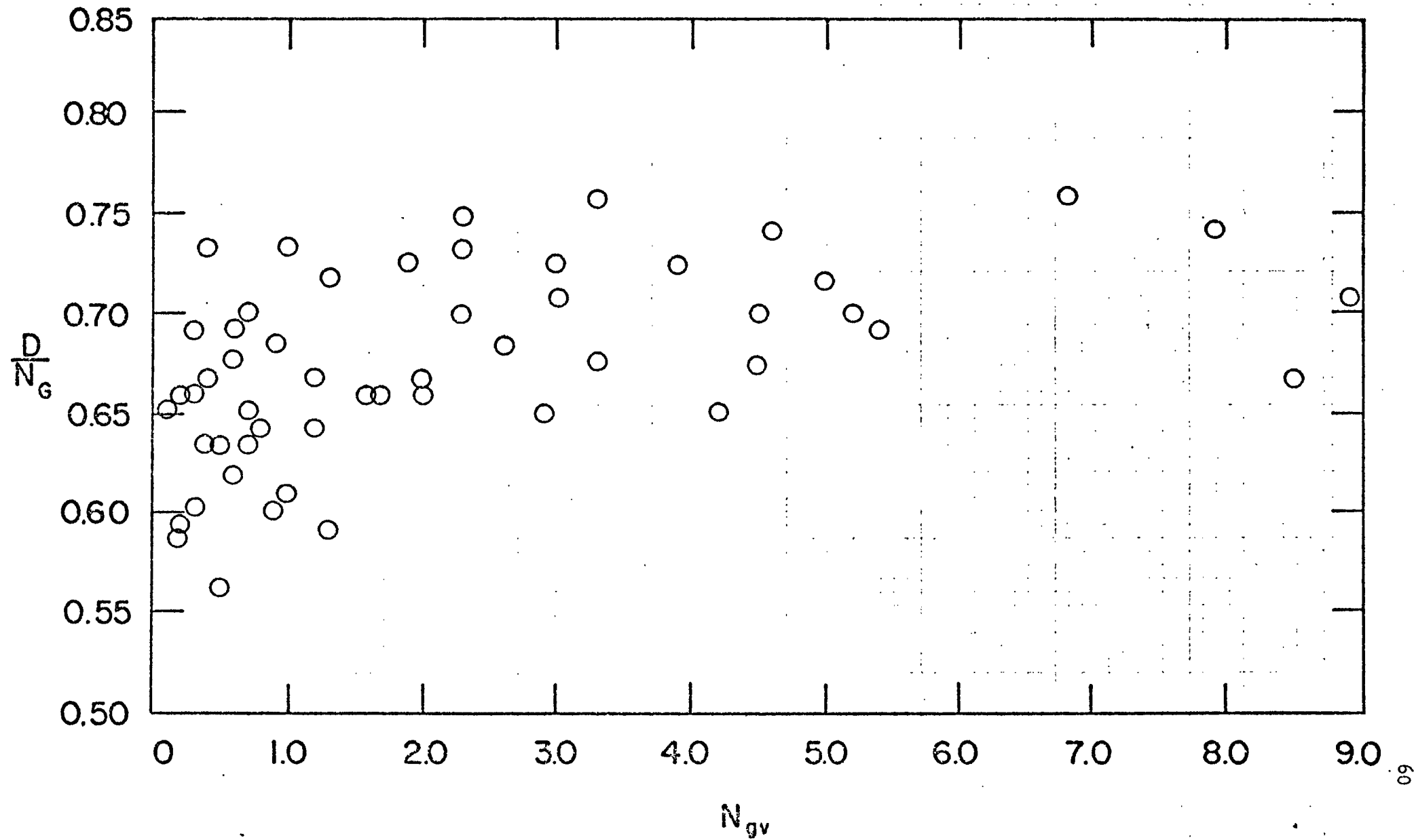


Figure 4.3-2. Effect of N_{gv} on Deformation Data: System B

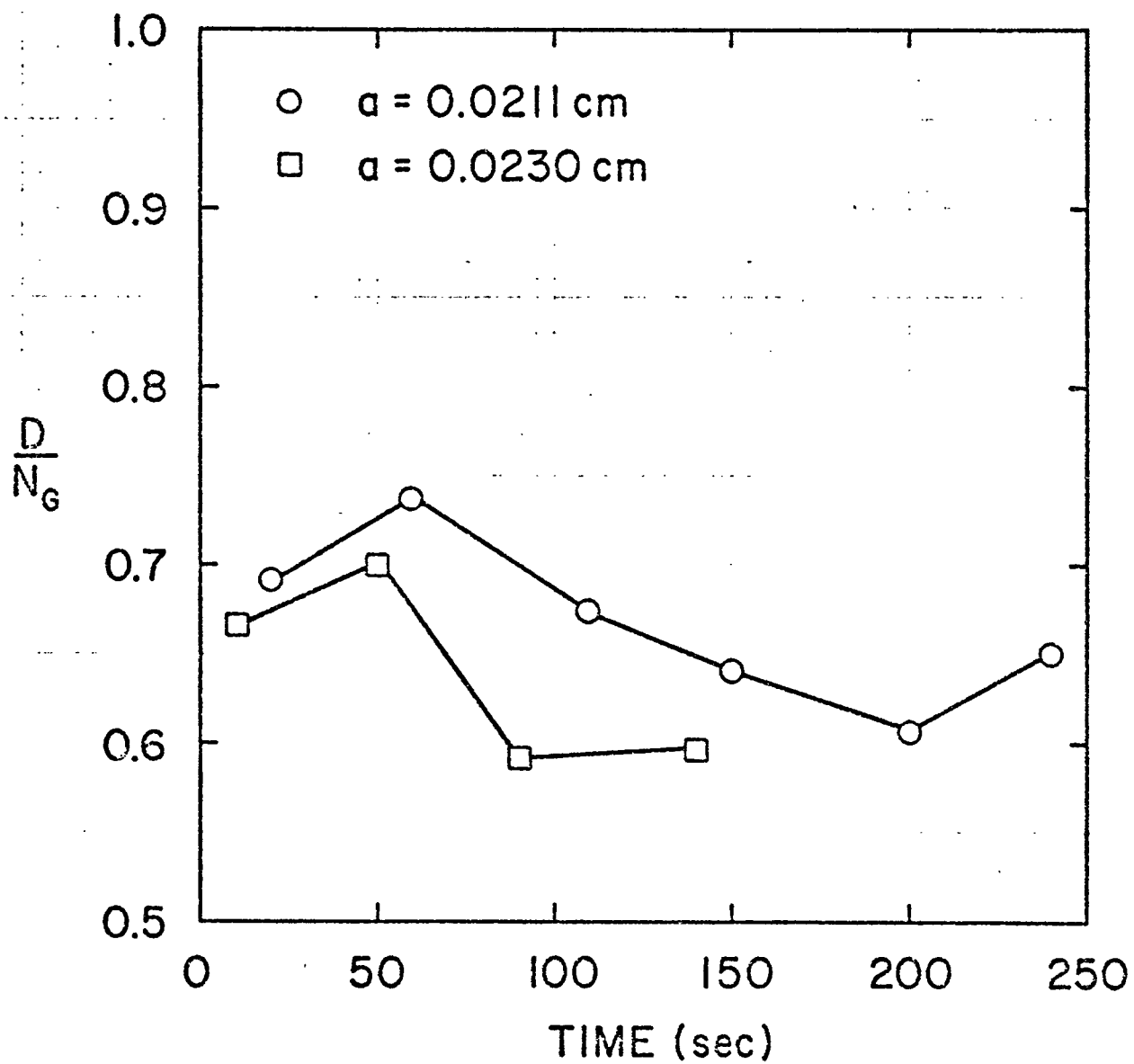


Figure 4.3-3. Time Dependence of Deformation: System B

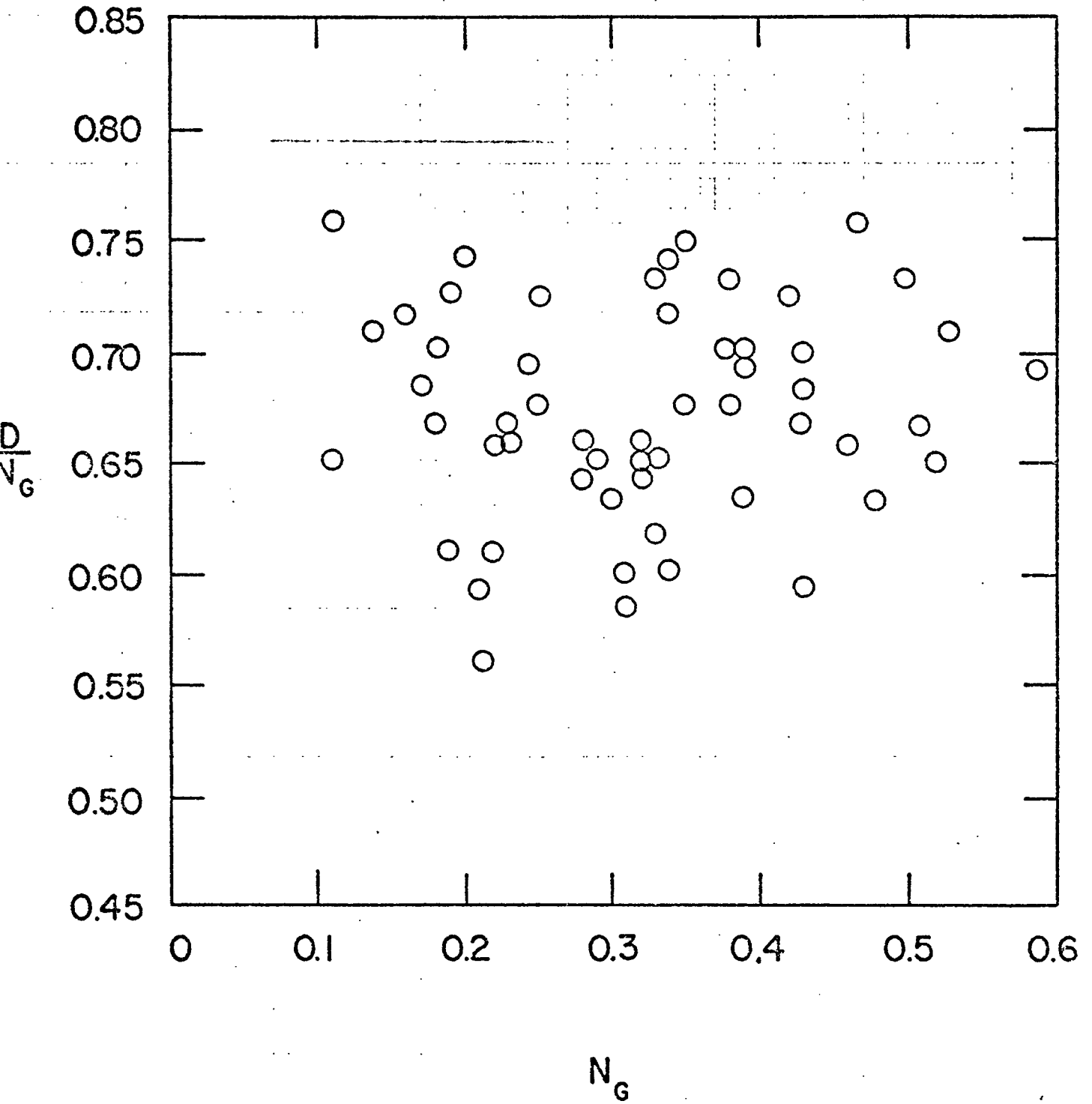


Figure 4.3-4. Effect of N_G on Deformation Data: System B

theoretical constraints were satisfied: 1) steady, incompressible flow, 2) Newtonian fluids, and 3) small Reynolds number. However, the criteria of small N_{gv} were not achieved for much of the data. To see if this had any effect on the results, the individual data points for D/N_G were plotted against N_{gv} in Figure 4.3-2. In general, the values of D/N_G for large N_{gv} showed little difference from those at small N_{gv} . If large N_{gv} had been important in altering the results, the values for D/N_G would be expected to become smaller as N_{gv} increased for the following reason. When gravitational forces are larger than viscous shear forces (large N_{gv}), the gravitational forces might be expected to make the drop more symmetric about the z axis, which would tend to decrease D. This effect apparently did not occur, so we may consider the N_{gv} criterion satisfied.

The dependence of D/N_G on time is shown in Figure 4.3-3. The individual data points for two drops is seen to be relatively unaffected by time, so the interfacial tension had presumably reached its equilibrium value. The deformation parameter D was less than 0.3 for most of the data.

As with System A, the data was analyzed by Equations (2.2-21) and (2.2-19). The validity of using Equation (2.2-21) instead of Eq. (2.2-13) needed to be checked since the values of N_G were as high as 0.5 for System B. Consequently the data was plotted in Figure 4.3-4 to see if D/N_G was dependent on N_G . Since D/N_G does not vary with N_G , Equation (2.2-21) was used in the analysis instead of Eq. (2.2-13).

The average values of D/N_G and λR for each drop were plotted in Figures 4.3-5 and 4.3-6, respectively. Equations (2.2-21) and (2.2-19) were used in an optimization of the data similarly to the System A data,

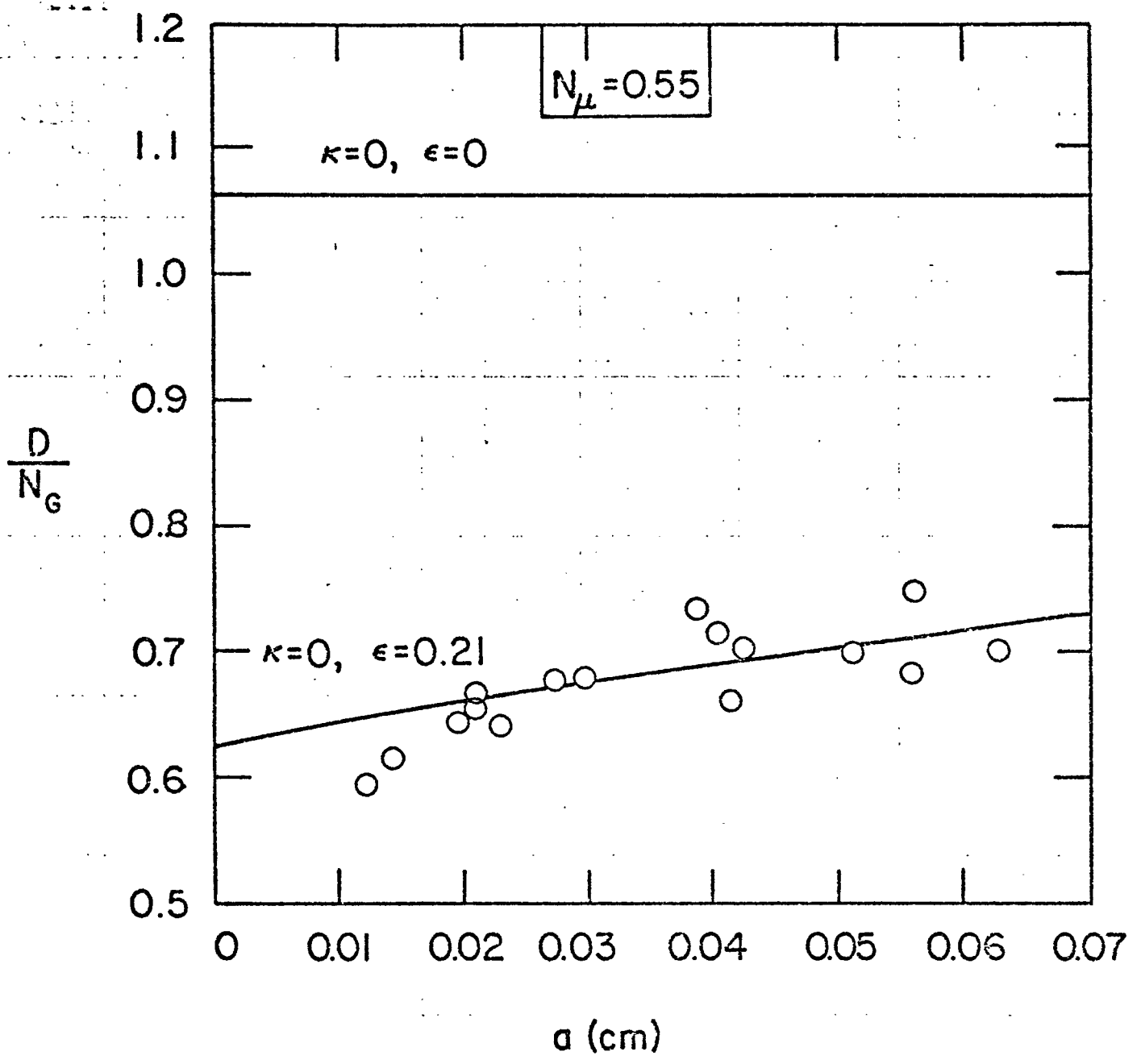


Figure 4.3-5. Deformation Data (D/N_G) and Fitted Curve: System B

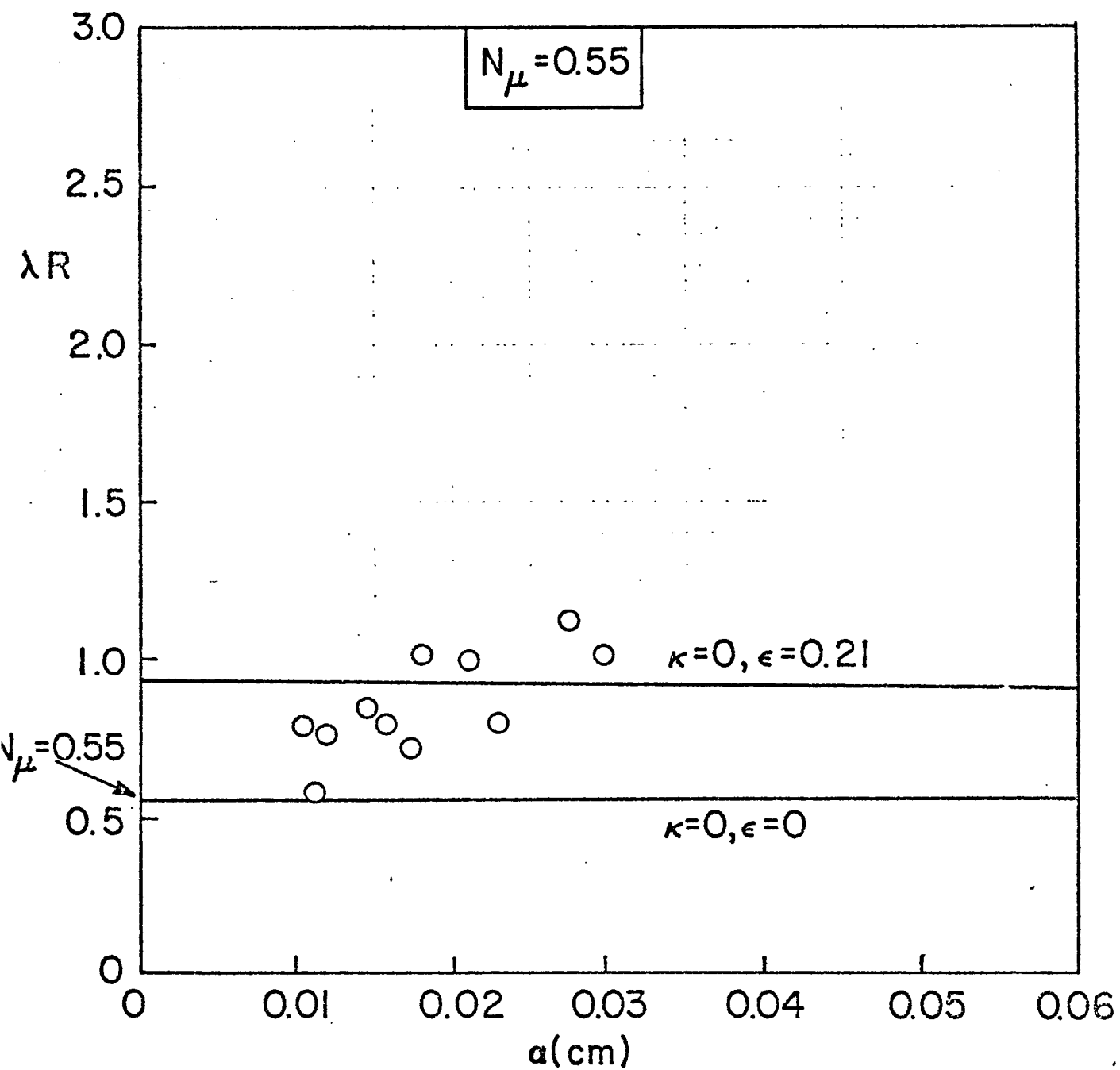


Figure 4.3-6. Deformation Data (λR) and Fitted Curve: System B

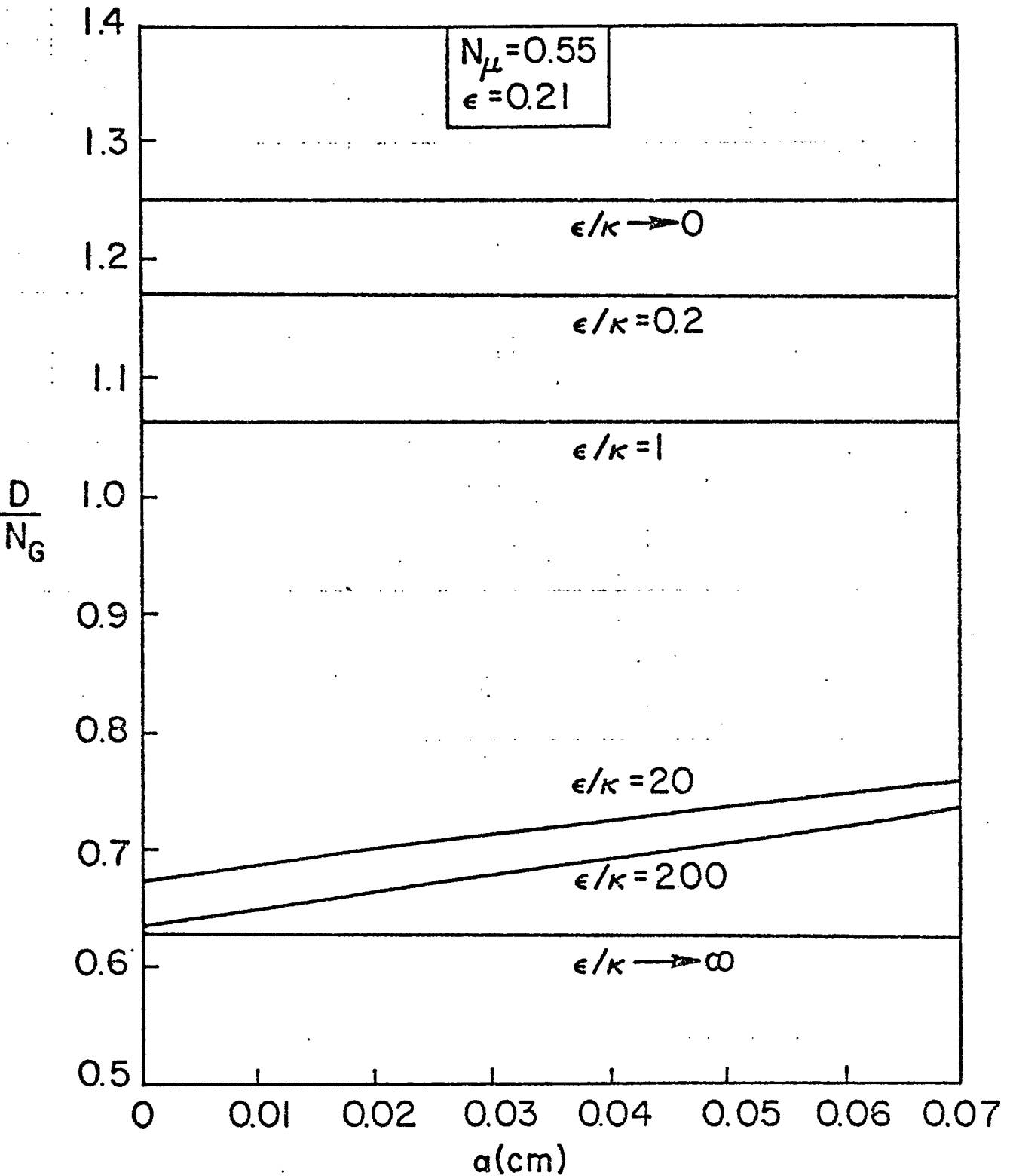


Figure 4.3-7. Deformations (D/N_G) for Various Values of ϵ/κ : System B

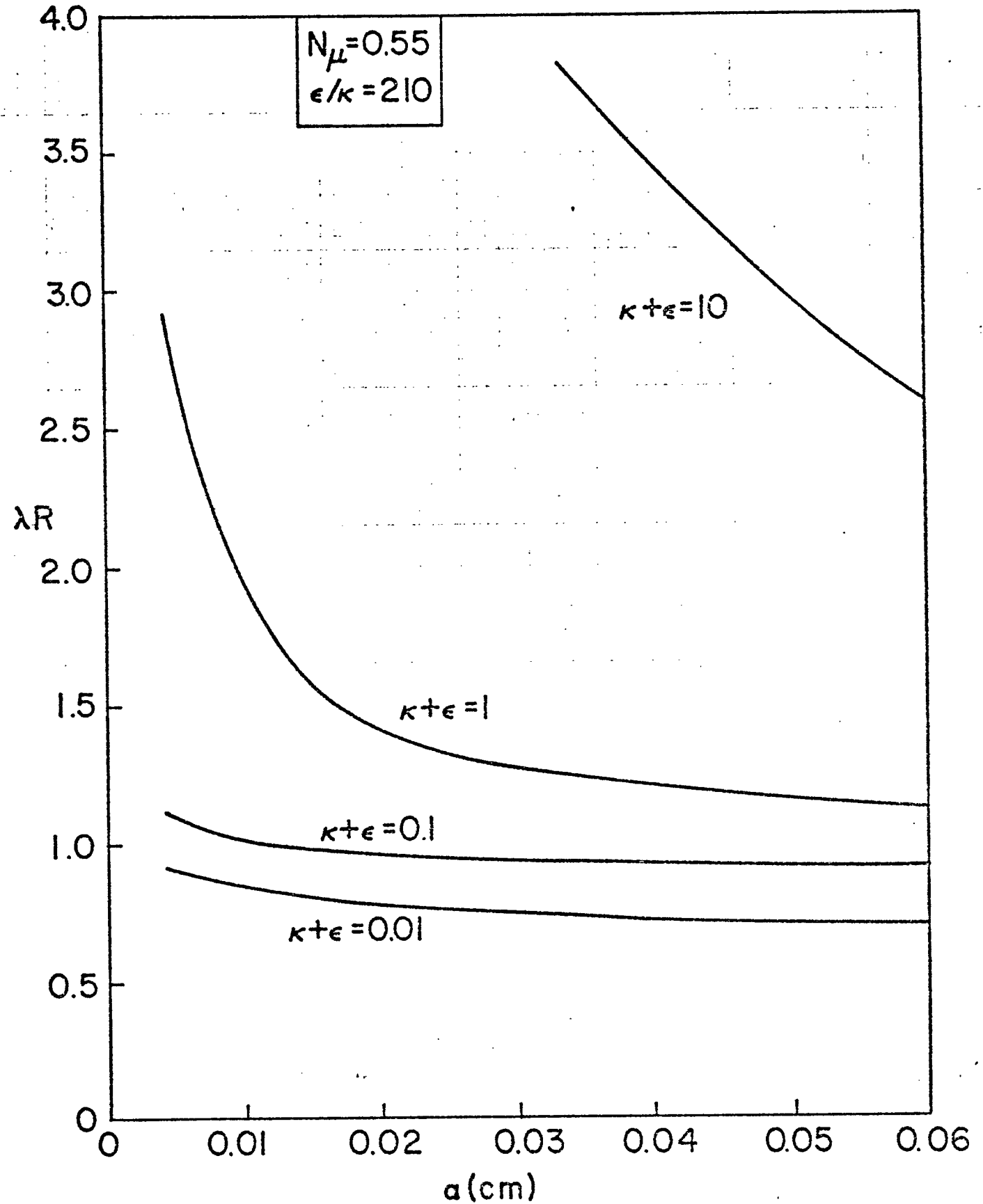


Figure 4.3-8. Values of λR , from Drop Deformations, for Various Values of $\kappa + \epsilon$: System B

and the values that gave the best fit of the data were $\kappa=0$ s.poise and $\epsilon=0.21$ s. poise. The D/N_G and λR equations were then graphed in the figures, using these values for κ and ϵ . Curves for κ and $\epsilon=0$ were also graphed to represent Taylor's predictions. Dynamic interfacial effects are evidently present in System B.

The sensitivity of the data to κ and ϵ was considered. A value of 0.001 s.poise was chosen to represent κ in these figures, instead of its value of zero, to make the calculations of ϵ/κ have real values. The value of ϵ/κ for the least squares minimized values, then, would be $0.21/0.001$, or 210. The curves for D/N_G and λR were graphed for various ϵ/κ and $(\kappa+\epsilon)$, respectively, in Figures 4.3-7 and 4.3-8.

The value of $\epsilon=0.21$ s.poise was held constant when ϵ/κ was varied in the D/N_G equation. When the experimental data of Figure 4.3-5 is compared with the curves of Figure 4.3-7, the ratio of ϵ to κ is somewhere between 100 and 500.

The ratio of $\epsilon/\kappa=210$ was held constant in the λR curves for various $(\kappa+\epsilon)$ in Figure 4.3-8. The data of Figure 4.3-6 would be in the range of $(\kappa+\epsilon)$ equal 0.01 to 0.4 s.poise.

Experimental errors could not change the data values enough to alter the previous conclusions to a substantial degree. The D/N_G data are clearly far away from the values associated with no dynamic interfacial behavior.

Interfacial tension gradients must be considered as well as the interfacial viscosities. If gradient effects were present, they would show up as a κ -type effect. Since the results clearly show that κ -type effects were negligible, we may conclude that interfacial tension gradients were absent in System B. This was to be expected since the value

of $(d\gamma/d \ln c_s)$ was rather small, as seen in Figure 4.3-1. And a small value of $(d\gamma/d \ln c_s)$ corresponds to a small N_{μ} .

Drop deformation results show that interfacial shear viscosity effects were present in System B. Any effects from the interfacial dilational viscosity or gradients of interfacial tension were apparently negligible.

The net effect of the dynamic interfacial phenomena is represented in Figure 4.3-9 by $\gamma_{\text{eff}}/\gamma$. This parameter rises from a value of about 1.5 at $a = 0.06$ cm to values near 1.8 as "a" decreases to about 0.01 cm. This representation illustrates that interfacial phenomena effects become increasingly important as the surface area to volume ratio of drops is increased.

Internal circulation experiments were also performed for System B. All theoretical constraints were met, including the stipulation of negligible deformation of the drops being tested.

The circulation data, m as a function of r_0 , were plotted in Figure 4.3-10. The curve for $\lambda=2.1$ (calculated from the equations of Torza, et al.) gave the best fit of the experimental data. This could represent values of $\kappa=0$ and $\epsilon=0.03$ s. poise for a drop radius of about 0.033 cm. The value of $\kappa=0$ was taken because of the conclusions from drop deformation. The curve for $\lambda=N_{\mu}$ was also drawn, representing κ and $\epsilon = 0$.

The λ curves are fairly sensitive in the region of $\lambda=2.1$, so the value of 2.1 must be in the neighborhood of the true value. Also, the experimental errors associated with m and r_0 are probably not great enough to account for the deviation of the data from the $\lambda=N_{\mu} = 0.55$ curve.

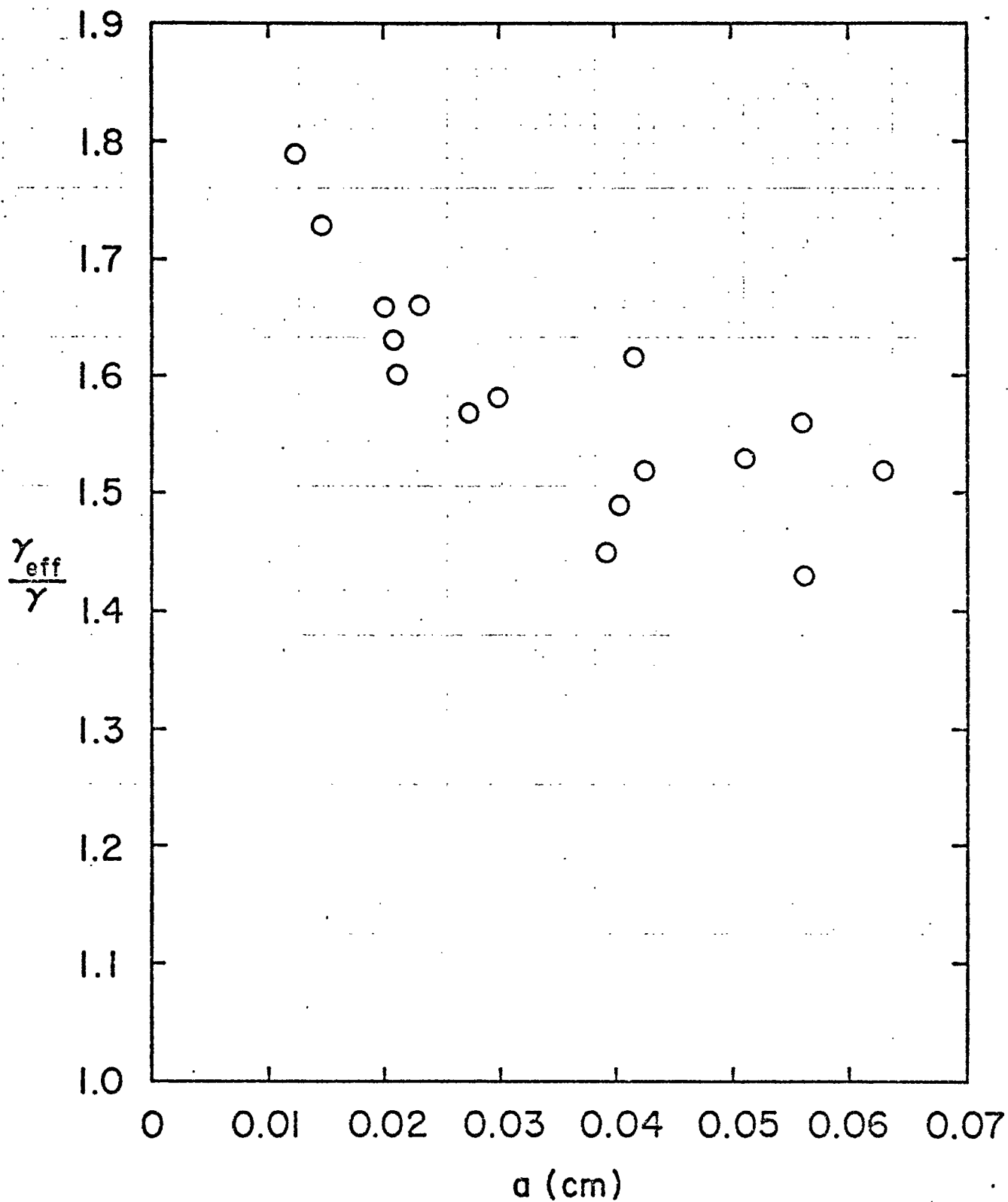


Figure 4.3-9. Data of γ_{eff}/γ from Drop Deformations: System B

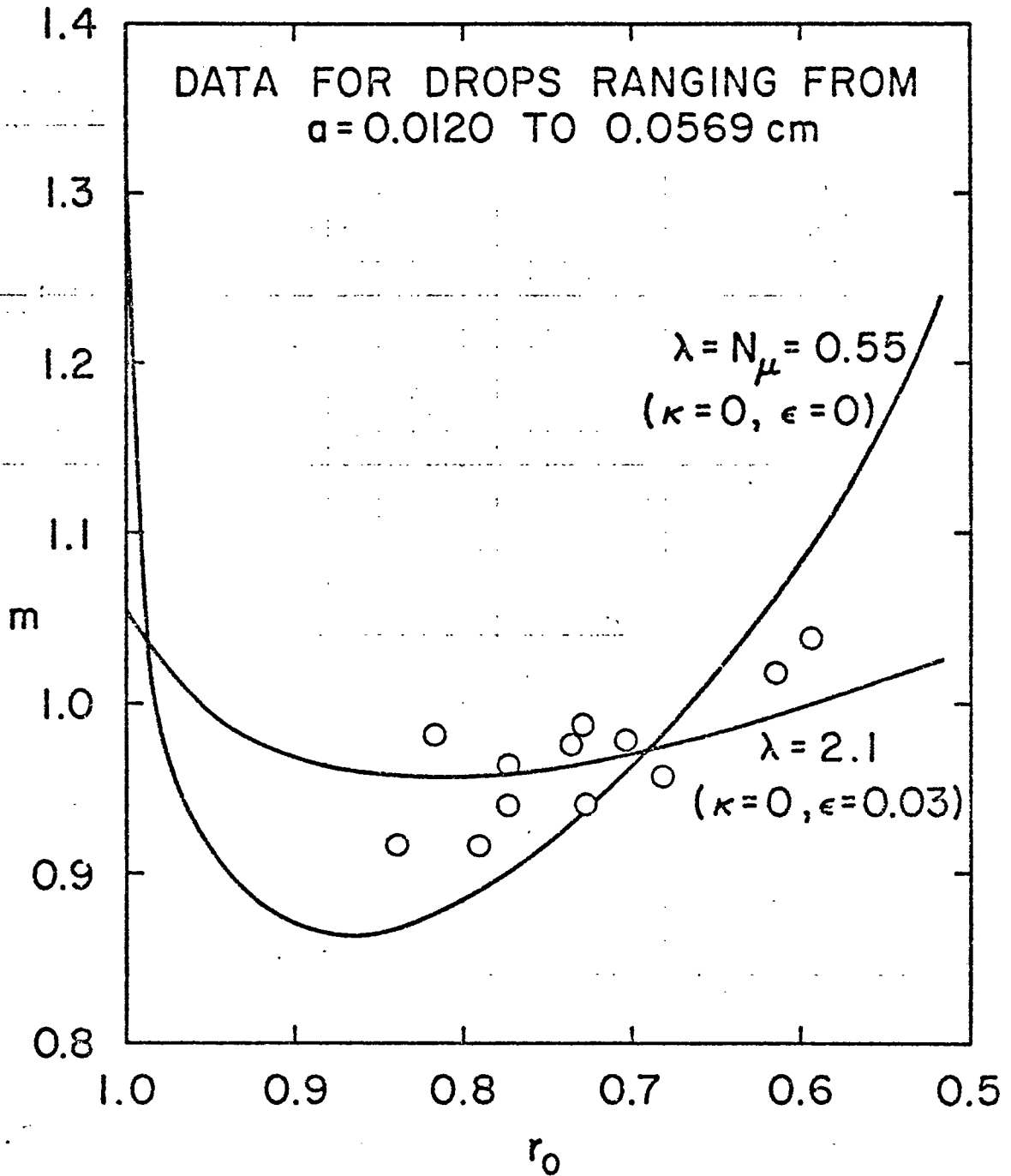


Figure 4.3-10. Experimental Internal Circulation Times and Fitted Curve: System B

Without the drop deformation results, the internal circulation results cannot distinguish between an effect caused by κ and ϵ . In addition, a κ -type effect could theoretically be caused by interfacial tension gradients, which would show up in the N_{κ} portion of $N_{\kappa+\epsilon}$.

To investigate this possibility, let us calculate the interfacial tension gradient necessary to completely stop internal circulation. Even though internal circulation was only partially inhibited in these experiments, these calculations will comparatively give an estimate of the force required to partially stop circulation.

For System B internal circulation studies, typical values for Ga were about $0.006 \text{ cm-sec}^{-1}$. For $\mu=0.4824$ poise, the force required to stop circulation becomes $0.0072 \text{ dyne-cm}^{-1}$ (using Equation 2.3-7). Instead of assuming a value for $1/k$ as was done for the System A calculations, $1/k$ will be found from the experimental data of γ versus c_s with the equation

$$\frac{1}{k} = \frac{d\gamma}{d \ln c_s} \quad (2.3-9)$$

The value for $(d\gamma/d \ln c_s)$ will be estimated from Figure 4.3-1. Since a smooth curve cannot be drawn through the γ data points to obtain a slope of $(d\gamma/d \ln c_s)$, the slope will be taken from the line segment with the greatest slope to obtain a maximum possible value of $(d\gamma/d \ln c_s)$. The slope of the segment between 0.0025 and 0.005 weight fraction of c_s is equal to $0.0043 \text{ dyne-cm}^{-1}$.

Substitution of the calculated force of $0.0072 \text{ dyne-cm}^{-1}$ and the value of $0.0043 \text{ dyne-cm}^{-1}$ for $1/k$ into Equation (2.3-8) yields $\Delta c/c=1.7$. This means that as an element of interface rotates over one quadrant and then the other quadrant of the drop's interface, a huge linear

compression and subsequent expansion of 170% would be required to totally stop internal circulation.

Although internal circulation did not totally stop in System B, we can comparatively estimate that the linear compression necessary to have impeded circulation would have been sizable, probably much more than the negligible amount observed from the experiments. These observations show that the likelihood of interfacial tension gradients is reduced when $(d\gamma/d \ln c_s)$ is small, as at large surfactant concentrations.

These internal circulation tests alone cannot distinguish between κ -type or ϵ effects. The foregoing calculations only suggest that interfacial tension gradients were negligible. At this point, the value of $\lambda=2.1$ could have been caused by either one of the interfacial viscosities.

A look at both the drop deformation and internal circulation results show dynamic interfacial forces. Deformation data demonstrably showed no κ -type effects at all, meaning both the interfacial dilational viscosity and interfacial tension gradients were negligible. The absence of interfacial tension gradients was also supported by the calculations done on the forces required to stop internal circulation. A value of $\epsilon=0.03$ s. poise would be calculated from $\lambda=2.1$ if $\kappa=0$. Drop deformation found a value of about 0.21 s. poise for ϵ . In any case, both sets of data show that the interfacial shear viscosity was non-zero in System B.

CHAPTER 5

CONCLUSIONS AND RECOMMENDATIONS

Dynamic interfacial phenomena were investigated by subjecting liquid drops to a simple shear field, which was generated by a Couette cylinder apparatus. Various studies of drop dynamics in such flow fields were made, including deformation tests, the position of the critical streamline (external to the drop), and the period of circulation around internal streamlines.

The major results and conclusions can be summarized:

1. A liquid-liquid system with no surfactant added was investigated. Significant dynamic interfacial behavior was observed, particularly in the internal circulation and the critical streamline experiments, in which the drop approached the behavior of a rigid body. Very large effects were caused by either the interfacial dilational viscosity (κ) or by interfacial tension gradients, which have similar effects as κ . The interfacial shear viscosity (ϵ) was also observed, but to a lesser degree. Values for these effects were approximately 3.33 surface poise for the κ -type effects, and 0.81 surface poise for the ϵ effect. Trace impurities that acted as surfactants may have been responsible for these results.
2. An investigation was also carried out on a surfactant, low interfacial tension system, that somewhat resembled the liquids encountered in micellar chemical flooding. High concentrations of surfactant were used to reduce the

possibility of developing interfacial tension gradients. Effects caused by either the interfacial dilational viscosity or interfacial tension gradients were apparently negligible, whereas the interfacial shear viscosity appeared to be in the range of 0.03 to 0.21 surface poise.

3. The experimental results and sample calculations have demonstrated the potential of very small surfactant concentrations, as of trace impurities, to cause significant dynamic interfacial behavior (from the development of interfacial tension gradients). Conversely, high concentration surfactant systems would decrease the chances of such effects occurring.
4. The deformation experiments are the only tests that can alone determine the individual contributions of the κ -type or ϵ effects. They are experimentally easier to run than the other methods used, but tend to be a little less accurate.
5. The internal circulation experiments, though more difficult to execute, are more sensitive to dynamic interfacial behavior than deformation tests, particularly the effects caused by interfacial tension gradients. Being a more sensitive method, internal circulation is a better test to study any behavior that changes with time.
6. The critical streamline experiments, besides being very sensitive, are more accurate than the other experimental methods carried out in this study. They are limited in use, however, since only a few particular liquid systems can naturally show the position of the critical streamlines of

drops. All other systems require the addition of dye or some other coloring agent to the continuous phase being tested.

These studies suggest the following extensions and recommendations for future work:

1. Increase the resemblance of test fluids to those used in micellar chemical flooding. One possibility is to work with water (plus added salt and surfactant) as the aqueous phase, and mineral oil and a co-solvent as the oil phase. The co-solvent would be added to make the two fluids almost neutrally buoyant. Another possibility is to use a polymer-thickened water solution (plus salt and surfactant) as the aqueous phase and mineral oil as the oil phase. The high viscosity of polymer-thickened water would decrease the settling velocity of the drop. Ultimately, crude oil could be tested in place of the mineral oil.
2. Run the deformation experiments at a higher shear rate (or higher capillary number N_G). This would emphasize the interfacial viscosity effects relative to the interfacial tension gradient effects. This would also increase the accuracy of the experiments in two ways. First, if N_G is large enough, then the deformation becomes independent of N_G . The latter is a function of the interfacial tension, which is difficult to determine accurately. Also, the geometric measurements of the deformation parameter and the orientation angle of the drop are more accurate when high N_G experiments cause large deformations.

3. Develop methods to view the critical streamline of drops in liquids where the critical streamline does not naturally show itself. Possibilities exist in the use of coloring agents, but they must be chosen with care so they will not act as surfactants or alter the liquids in some other way.
4. Run transient deformation experiments, which would offer a new way of determining the dynamic interfacial properties. Also, oscillatory tests could be developed to see if elastic forces exist on the interface.

BIBLIOGRAPHY

1. Ball, W. E., "BSOLVE: Solution to a Set of Nonlinear Equations by Marquardt's Method." Washington University.
2. Boussinesq, J., Amer. Chem. Phys., 29, 349 (1913).
3. Cox, R. G., J. Fluid Mech., 37, 601 (1969).
4. Flumerfelt, R. W., "Effects of Surface Active Agents on the Hydrodynamic Behavior of Drops in a General Flow Field." Univ. of Houston, 1977.
5. Flumerfelt, R. W., "Effects of Surface Viscosities on the Deformation and Circulation of Drops in Shear Fields." Submitted to J. Colloid Sci., 1977.
6. Gibbs, J. W., "On the Equilibrium of Heterogeneous Substances." Trans. Conn. Acad., 3, 343 (1878).
7. Mayer, E., "The Inference of Interfacial Properties from Capillary Waves." Ph.D. Thesis, Univ. of Delaware, 1969.
8. Oldroyd, J., Proc. Roy. Soc., A-232, 567 (1955).
9. Phillips, W. J., "Dynamic Interfacial Properties at Liquid-Liquid Interfaces." M. S. Thesis, Univ. of Houston, 1977.
10. Rumscheidt, F. D. and S. G. Mason, J. Colloid Sci., 16, 238 (1961).
11. Scriven, L. E., Chem. Engr. Sci., 12, 98 (1960).
12. Slattery, J. C., A.I.Ch.E. J., 20, 1145 (1974).
13. Slattery, J. C., Chem. Engr. Sci., 19, 379 (1964).
14. Slattery, J. C., IEC Fundamentals, 6, 108 (1967); *ibid.* 7, 672 (1968).
15. Tavgac, T., "Drop Deformation and Breakup in Simple Shear Fields." Ph.D. Thesis, Univ. of Houston, 1972.
16. Taylor, G. I., Proc. Roy. Soc., Ser. A, 138, 41 (1932).
17. Taylor, G. I., Proc. Roy. Soc., Ser. A., 146, 501 (1934).
18. Torza, S., C. P. Henry, R. G. Cox, and S. G. Mason, J. Colloid and Interface Sci., 35, 529 (1971).
19. Wei, L., W. Schmidt, and J. C. Slattery, "Measurement of the Surface Dilational Viscosity." Northwestern Univ., 1973.

APPENDIX I
EXPERIMENTAL DATA

Original data and calculated variables from the Couette experiments, along with interfacial tension tests for System B, are given in the following tables.

For each drop, the D/N_G and λR data were each averaged to obtain the value of D/N_G (avg) and λR (avg), respectively. The variable $\gamma_{\text{eff}}/\gamma$ was evaluated from D/N_G (avg). Some of the drops decreased in size during the course of the experiment, thus accounting for the difference in "a" values for those drops.

Table 1-1
DEFORMATION DATA FOR SYSTEM A

a (cm)	G (sec ⁻¹)	N _{gv}	D	N _G	D/N _G	Time (sec)
0.0438	9.31	0.0443	0.0765	0.0744	1.029	
0.0435	9.44	0.0434	0.0827	0.0751	1.101	
"	9.01	0.0427	0.0809	0.0764	1.060	
"	9.02	0.0455	0.0737	0.0717	1.028	
"	10.03	0.0409	0.0885	0.0797	1.110	
"	9.40	0.0436	0.0761	0.0747	1.019	
0.0433	9.78	0.0417	0.0794	0.0774	1.026	
0.0431	9.86	0.0411	0.0928	0.0776	1.197	

$$D/N_G \text{ (avg)} = 1.07$$

$$\gamma_{\text{eff}}/\gamma = 0.935$$

0.0509	8.52	0.0563	0.0863	0.0792	1.090	
"	9.19	0.0522	0.0955	0.0854	1.118	
"	7.60	0.0631	0.0812	0.0706	1.150	
"	9.77	0.0491	0.1043	0.0908	1.149	
0.0506	9.99	0.0477	0.1028	0.0924	1.112	
0.0506	9.54	0.0500	0.0973	0.0882	1.103	

$$D/N_G \text{ (avg)} = 1.12$$

$$\gamma_{\text{eff}}/\gamma = 0.893$$

0.0562	6.72	0.0789	0.0864	0.0690	1.252	36
0.0555	8.08	0.0646	0.0943	0.0819	1.151	240
0.0552	9.29	0.0560	0.1091	0.0937	1.165	500
"	9.75	0.0533	0.1136	0.0983	1.156	700
0.0550	9.46	0.0547	0.1193	0.0950	1.255	1000
"	7.97	0.0649	0.1096	0.0800	1.370	1500
"	9.72	0.0533	0.1167	0.0975	1.197	1850
"	9.51	0.0544	0.1198	0.0954	1.255	2100
"	9.56	0.0542	0.1156	0.0959	1.206	2500
0.0554	7.61	0.0674	0.1038	0.0757	1.371	2850

$$D/N_G \text{ (avg)} = 1.24$$

$$\gamma_{\text{eff}}/\gamma = 0.805$$

a (cm)	G (sec ⁻¹)	N _{gv}	D	N _G	D/N _G	Time (sec)
0.0563	9.55	0.0556	0.1042	0.0982	1.060	
"	9.18	0.0578	0.1029	0.0944	1.090	
"	8.16	0.0650	0.0943	0.0840	1.122	
"	8.63	0.0615	0.0905	0.0888	1.019	
"	9.36	0.0567	0.1070	0.0963	1.111	
"	9.79	0.0542	0.1111	0.1007	1.103	
"	9.18	0.0578	0.0965	0.0945	1.022	
"	8.96	0.0592	0.1006	0.0922	1.091	
"	9.97	0.0532	0.1074	0.1026	1.047	

$$D/N_G (\text{avg}) = 1.07$$

$$\gamma_{\text{eff}}/\gamma = 0.935$$

0.0714	6.77	0.0994	0.0933	0.0884	1.056	
"	8.79	0.0766	0.1278	0.1147	1.114	
"	9.27	0.0726	0.1266	0.1209	1.047	
0.0711	7.90	0.0848	0.1082	0.1026	1.054	
"	8.66	0.0774	0.1189	0.0125	1.058	
"	8.41	0.0797	0.1170	0.0922	1.071	
0.0708	8.65	0.0771	0.1195	0.118	1.068	

$$D/N_G (\text{avg}) = 1.07$$

$$\gamma_{\text{eff}}/\gamma = 0.935$$

0.0870	5.08	0.1615	0.1011	0.0807	1.254	175
"	5.48	0.1496	0.1087	0.0871	1.249	350
"	4.89	0.1676	0.0963	0.0777	1.239	720
"	5.37	0.1528	0.1099	0.0853	1.289	1000
"	8.06	0.1472	0.1444	0.1281	1.127	1350
"	7.78	0.1067	0.1398	0.1220	1.146	1500
"	7.74	0.1059	0.1354	0.1229	1.102	1600
0.0866	8.96	0.0910	0.1719	0.1416	1.214	1700

$$D/N_G (\text{avg}) = 1.20$$

$$\gamma_{\text{eff}}/\gamma = 0.833$$

0.0920	6.31	0.1373	0.1171	0.1062	1.103	
"	7.00	0.1247	0.1443	0.1169	1.234	
"	7.25	0.1196	0.1520	0.1219	1.247	
"	7.22	0.1200	0.1415	0.1215	1.165	
0.0916	8.51	0.1013	0.1610	0.1424	1.130	
"	8.08	0.1068	0.1589	0.1352	1.176	
"	7.94	0.1086	0.1576	0.1328	1.187	
"	8.50	0.1015	0.1794	0.1422	1.261	

$$D/N_G (\text{avg}) = 1.19$$

$$\gamma_{\text{eff}}/\gamma = 0.840$$

a (cm)	G (sec ⁻¹)	N _{gv}	D	N _G	D/N _G	Time (sec)
0.1186	4.16	0.2685	0.1282	0.0901	1.422	
"	4.94	0.2263	0.1350	0.1070	1.262	
"	5.15	0.2169	0.1407	0.1116	1.261	
"	5.57	0.2007	0.1456	0.1206	1.207	
"	5.92	0.1887	0.1577	0.1283	1.229	
"	6.25	0.1788	0.1569	0.1354	1.159	
"	6.28	0.1778	0.1692	0.1361	1.243	
"	5.88	0.1901	0.1628	0.1273	1.279	

$$D/N_G \text{ (avg)} = 1.26$$

$$\eta_{\text{eff}}/\eta = 0.794$$

a (cm)	α (deg)	N _G	λ_R	λ_R (avg)
0.0448	47.5	0.0744	1.238	
0.0435	52.5	0.0751	3.595	
0.0435	49.5	0.0764	2.147	
0.0435	46.5	0.0717	0.770	1.87
0.0435	46.5	0.0797	0.693	
0.0433	46.5	0.0774	0.713	
0.0431	53.5	0.0776	3.918	
0.0509	48.5	0.0792	1.616	
"	49.5	0.0854	1.920	
"	51.5	0.0706	3.329	
"	55.5	0.0908	4.075	3.07
0.0506	53.5	0.0924	3.290	
0.0506	55.5	0.0882	4.195	
0.0562	48.5	0.0690	1.855	
0.0555	47.5	0.0819	1.125	
0.0552	47.5	0.0937	0.983	
0.0552	48.5	0.0983	1.302	
0.0550	50.5	0.0950	2.105	1.51
"	48.5	0.0800	1.600	
"	46.5	0.0975	0.566	
"	48.5	0.0954	1.342	
"	50.5	0.0959	2.086	
0.0544	49.5	0.0757	2.166	
0.0563	47.5	0.0982	0.938	
"	49.5	0.0944	1.737	
"	46.5	0.0840	0.657	0.92
"	48.5	0.0888	1.441	
"	45.5	0.0963	0.191	
"	46.5	0.1007	0.546	

<u>a (cm)</u>	<u>α (deg)</u>	<u>N_G</u>	<u>λR</u>	<u>λR (avg)</u>
0.0687	48.5	0.0735	1.741	
"	50.5	0.0671	2.981	
"	52.5	0.0767	3.520	
"	49.5	0.0737	2.225	
"	48.5	0.0627	2.041	1.85
"	47.5	0.0683	1.348	
"	48.5	0.0874	1.465	
"	46.5	0.0756	0.730	
"	49.5	0.0749	2.189	
0.0681	48.5	0.0594	2.155	
0.0714	51.5	0.0884	2.658	
"	55.5	0.1111	3.333	
"	55.5	0.1147	3.217	
"	49.5	0.1209	1.355	
"	48.5	0.1109	1.153	2.25
0.0711	48.5	0.1026	1.243	
"	51.5	0.1125	2.080	
"	53.5	0.1092	2.789	
0.0708	52.5	0.1118	2.411	
0.0920	49.5	0.1062	1.547	
"	53.5	0.1169	2.598	
"	53.5	0.1219	2.492	
"	52.5	0.1214	2.213	2.17
0.0916	53.5	0.1424	2.141	
"	50.5	0.1352	1.481	
"	55.5	0.1328	2.782	
"	53.5	0.1422	2.141	
0.1186	53.5	0.1070	2.841	
"	55.5	0.1116	3.304	
"	55.5	0.1206	3.058	
"	55.5	0.1283	2.891	3.16
"	58.5	0.1305	3.437	
"	58.5	0.1361	3.412	
"	56.5	0.1274	3.165	

Table 1-2
INTERNAL CIRCULATION DATA FOR SYSTEM A

<u>a (cm)</u>	<u>G (sec⁻¹)</u>	<u>T (sec)</u>	<u>r_o</u>	<u>m</u>
0.0679	0.385	32.8	0.144	1.005
0.054	0.390	31.7	0.225	0.984
0.0542	0.0501	250.0	0.230	0.997
0.0542	0.168	74.5	0.254	0.996
0.0568	1.860	6.81	0.291	1.008
0.0538	0.105	117.1	0.315	0.978
0.0679	0.385	32.8	0.506	1.005
0.0521	0.618	20.2	0.620	0.993
0.0521	0.618	20.2	0.630	0.993
0.0542	0.150	84.9	0.632	1.013
0.0542	0.390	31.7	0.708	0.984
0.0542	0.390	31.7	0.709	0.984
0.0542	0.168	74.5	0.851	0.996

Table 1-3
CRITICAL STREAMLINE DATA FOR SYSTEM A

<u>a (cm)</u>	<u>G (sec⁻¹)</u>	<u>x*</u>	<u>y*</u>
0.0900	3.165	1.137	0
		1.05	0.27
		0.94	0.55
		0.76	0.82
		0.56	1.09
		0.42	1.27
		0.34	1.45
		0.27	1.64
		0.22	1.82

<u>a (cm)</u>	<u>G (sec⁻¹)</u>	<u>x*</u>	<u>y*</u>
0.0652	4.651	1.143	0
		1.08	0.41
		0.93	0.75
		0.72	0.99
		0.52	1.30
		0.36	1.51
0.0652	2.729	1.150	0
		1.13	0.28
		1.09	0.56
		0.94	0.83
		0.66	1.11
		0.51	1.25
		0.43	1.39
		0.29	1.67
		0.21	1.94

Table I-4

DEFORMATION DATA FOR SYSTEM B

<u>a (cm)</u>	<u>G (sec⁻¹)</u>	<u>N_{gv}</u>	<u>D</u>	<u>N_G</u>	<u>D/N_G</u>	<u>Time (sec)</u>
0.0123	2.58	0.391	0.107	0.194	0.553	
"	4.17	0.242	0.183	0.313	0.584	
"	6.93	0.145	0.337	0.521	0.647	

$$D/N_G \text{ (avg)} = 0.595$$

$$\gamma_{\text{eff}}/\gamma = 1.79$$

0.0146	5.12	0.233	0.301	0.455	0.661	
"	3.59	0.333	0.210	0.319	0.659	
"	2.46	0.484	0.123	0.219	0.560	
"	3.80	0.314	0.203	0.338	0.600	
"	4.85	0.246	0.256	0.431	0.594	

$$D/N_G \text{ (avg)} = 0.615$$

$$\gamma_{\text{eff}}/\gamma = 1.73$$

0.0200	1.58	1.041	0.118	0.193	0.612	
"	2.47	0.665	0.192	0.302	0.636	
"	3.20	0.514	0.246	0.391	0.630	
"	4.16	0.395	0.340	0.509	0.669	
"	5.09	0.323	0.430	0.622	0.690	
"	3.95	0.416	0.305	0.483	0.630	
"	2.67	0.614	0.202	0.327	0.616	

$$D/N_G \text{ (avg)} = 0.641$$

$$\gamma_{\text{eff}}/\gamma = 1.66$$

0.0209	2.49	0.687	0.208	0.318	0.654	
--------	------	-------	-------	-------	-------	--

$$D/N_G \text{ (avg)} = 0.654$$

$$\gamma_{\text{eff}}/\gamma = 1.63$$

<u>a (cm)</u>	<u>G (sec⁻¹)</u>	<u>N_{gv}</u>	<u>D</u>	<u>N_G</u>	<u>D/N_G</u>	<u>Time (sec)</u>
0.0211	3.05	0.566	0.272	0.393	0.692	20
"	3.92	0.441	0.371	0.505	0.735	60
"	2.94	0.586	0.256	0.379	0.675	110
"	2.17	0.797	0.179	0.280	0.640	150
"	1.67	1.035	0.130	0.215	0.606	200
"	2.56	0.677	0.215	0.330	0.652	240

$$D/N_G \text{ (avg)} = 0.667$$

$$\gamma_{\text{eff}}/\gamma = 1.60$$

0.0230	1.60	1.179	0.150	0.225	0.667	10
"	2.72	0.693	0.269	0.383	0.701	50
"	1.49	1.270	0.124	0.209	0.592	90
"	2,21	0.854	0.186	0.311	0.598	140

$$D/N_G \text{ (avg)} = 0.640$$

$$\gamma_{\text{eff}}/\gamma = 1.66$$

0.0274	1.35	1.666	0.148	0.226	0.657
"	1.93	1.162	0.207	0.323	0.641
"	2.24	1.002	0.276	0.375	0.736
"	2.59	0.866	0.295	0.434	0.680

$$D/N_G \text{ (avg)} = 0.678$$

$$\gamma_{\text{eff}}/\gamma = 1.57$$

0.0297	0.58	4.193	0.068	0.105	0.651
"	0.93	2.623	0.115	0.168	0.684
"	1.23	1.972	0.148	0.223	0.661
"	1.52	1.600	0.182	0.275	0.661
"	1.86	1.310	0.240	0.336	0.715

$$D/N_G \text{ (avg)} = 0.674$$

$$\gamma_{\text{eff}}/\gamma = 1.58$$

0.0388	0.47	6.812	0.084	0.111	0.761
"	0.82	3.901	0.140	0.193	0.726
"	1.07	2.984	0.183	0.252	0.725
"	1.37	2.315	0.239	0.325	0.733

$$D/N_G \text{ (avg)} = 0.736$$

$$\gamma_{\text{eff}}/\gamma = 1.45$$

<u>a (cm)</u>	<u>G (sec⁻¹)</u>	<u>N_{gv}</u>	<u>D</u>	<u>N_G</u>	<u>D/N_G</u>	<u>Time (sec)</u>
0.0406	0.66	5.031	0.117	0.164	0.714	
"	1.02	3.271	0.170	0.252	0.674	
"	1.42	2.349	0.263	0.351	0.750	
"	1.71	1.947	0.307	0.424	0.725	

$$D/N_G \text{ (avg)} = 0.716$$

$$\gamma_{\text{eff}}/\gamma = 1.49$$

0.0416	1.16	2.944	0.190	0.294	0.648	
"	1.71	1.989	0.290	0.434	0.668	

$$D/N_G \text{ (avg)} = 0.658$$

$$\gamma_{\text{eff}}/\gamma = 1.62$$

0.0426	0.67	5.184	0.123	0.175	0.703	
"	1.52	2.305	0.277	0.394	0.702	

$$D/N_G \text{ (avg)} = 0.703$$

$$\gamma_{\text{eff}}/\gamma = 1.51$$

0.0511	0.46	9.022	0.102	0.145	0.704	
"	0.78	5.352	0.168	0.244	0.689	

$$D/N_G \text{ (avg)} = 0.697$$

$$\gamma_{\text{eff}}/\gamma = 1.53$$

0.0559	0.54	8.504	0.123	0.184	0.668	
"	1.02	4.497	0.234	0.347	0.675	
"	1.55	2.953	0.374	0.529	0.707	

$$D/N_G \text{ (avg)} = 0.683$$

$$\gamma_{\text{eff}}/\gamma = 1.56$$

0.0559	0.58	7.852	0.147	0.199	0.738	
"	1.00	4.567	0.254	0.342	0.744	
"	1.37	3.348	0.353	0.466	0.756	

$$D/N_G \text{ (avg)} = 0.746$$

$$\gamma_{\text{eff}}/\gamma = 1.43$$

<u>a (cm)</u>	<u>G (sec⁻¹)</u>	<u>N_{gv}</u>	<u>D</u>	<u>N_G</u>	<u>D/N_G</u>	<u>Time (sec)</u>
0.0627	1.131	4.544	0.303	0.433	0.100	

$$D/N_G (\text{avg}) = 0.700$$

$$\gamma_{\text{eff}}/\gamma = 1.52$$

<u>a (cm)</u>	<u>α (deg)</u>	<u>N_G</u>	<u>λR</u>	<u>λR (avg)</u>
0.0104	49.5	0.143	1.168	
"	51.0	0.190	1.179	
"	49.5	0.220	0.673	0.780
"	48.0	0.266	0.417	
"	50.5	0.326	0.629	
"	50.0	0.304	0.612	
0.0114	50.0	0.314	0.592	
"	51.0	0.437	0.513	0.553
0.0123	49.5	0.194	0.861	
"	50.0	0.313	0.594	0.771
"	56.5	0.521	0.858	
0.0146	58.5	0.455	1.178	
"	53.0	0.319	0.947	
"	47.5	0.219	0.421	0.844
"	52.5	0.338	0.834	
"	54.5	0.431	0.840	
0.0160	51.0	0.306	0.732	
"	56.5	0.427	1.047	
"	59.0	0.521	1.075	
"	55.5	0.404	1.000	0.796
"	52.0	0.351	0.746	
"	49.0	0.298	0.497	
"	48.5	0.271	0.476	
0.0174	47.5	0.188	0.490	
"	51.5	0.261	0.931	0.704
"	51.0	0.324	0.691	
0.0180	52.0	0.240	1.095	
"	53.5	0.351	0.917	1.006
0.0211	57.0	0.393	1.193	
"	56.5	0.379	1.199	
"	53.5	0.280	1.150	0.982
"	48.0	0.215	0.516	
"	52.5	0.330	0.854	

<u>a (cm)</u>	<u>α (deg)</u>	<u>N_G</u>	<u>λ_R</u>	<u>λ_R (avg)</u>
0.0230	56.0	0.383	1.110	0.795
"	48.5	0.209	0.617	
"	50.5	0.311	0.659	
0.0274	54.5	0.323	1.121	1.151
"	58.0	0.434	1.182	
0.0297	52.5	0.275	1.025	1.021
"	54.0	0.336	1.018	

Table 1-5
INTERNAL CIRCULATION DATA FOR SYSTEM B

<u>a (cm)</u>	<u>G (sec⁻¹)</u>	<u>T (sec)</u>	<u>r_o</u>	<u>m</u>
0.0124	0.226	57.6	0.594	1.036
0.0569	0.102	125.7	0.614	1.026
0.0396	0.191	63.3	0.684	0.962
0.0120	0.494	24.9	0.703	0.979
0.0456	0.086	137.6	0.727	0.941
0.0124	0.472	26.3	0.729	0.988
0.0163	0.392	31.3	0.734	0.976
0.0163	0.392	30.9	0.773	0.964
0.0176	0.475	24.9	0.775	0.941
0.0398	0.199	57.8	0.791	0.915
0.0225	0.166	74.8	0.818	0.988
0.0398	0.204	56.4	0.838	0.915

Table 1-6
INTERFACIAL TENSION FOR SYSTEM B

γ ($\frac{\text{dyne}}{\text{cm}}$)	c_s (weight fraction)
0.077	0.001
0.078	0.0025
0.082	0.005
0.079	0.010
0.080	0.015
0.079	0.02

APPENDIX II
ERROR ANALYSIS

Errors in geometric, kinematic and physical property measurements, and derived dimensionless groups are summarized in Table II-1. The standard deviations for experimental data measurements were calculated from

$$s_u = \left[\frac{\sum_{j=1}^n (X_j - \bar{X})^2}{n-1} \right]^{1/2} \quad (11-1)$$

where n is the number of data X_j , and \bar{X} is the average of all measurements. The standard deviations of the derived data groups were calculated from

$$s_f = \left[\sum_{i=1}^N \left(\frac{\partial f(u_i)}{\partial u_i} s_{u_i} \right)^2 \right]^{1/2} \quad (11-2)$$

where $f(u_i)$ is a derived group as a function of its N variables u_i . The quantities s_{u_i} are the standard deviations for the experimental data measurements, as calculated from Equation (11-1). The assumption of Equation (11-2) is that all errors are random and follow Gaussian distributions.

Table II-1
SUMMARY OF DATA ERRORS

<u>Quantity</u>	<u>Standard Deviation</u>	<u>Notes</u>
a	0.6 %	Evaluated from 11 randomly chosen data
B	0.4 %	Evaluated from 21 randomly chosen data
G	0.2 %	Evaluated from 22 randomly chosen data
L	0.4 %	Evaluated from 21 randomly chosen data
T	5.2 %	Evaluated from 9 randomly chosen data
α (Sys. A)	7.3 %	Evaluated from 27 randomly chosen data
α (Sys. B)	3.4 %	Evaluated from 27 randomly chosen data
γ	6.6 %	Evaluated from 12 randomly chosen data
μ	0.6 %	Evaluated from 8 randomly chosen data
ρ	<0.1 %	Evaluated from 6 randomly chosen data
D	2.4 %	$\frac{L - B}{L + B}$
D/N_G	7.1 %	$\frac{D}{N_G}$
m	5.2 %	$\frac{TG}{4\pi}$
N_G	6.7 %	$\frac{\mu Ga}{\gamma}$
r_o	4.3 %	Evaluated from 14 randomly chosen data
x^*	3.6 %	Evaluated from 9 randomly chosen data
y^*	3.6 %	Evaluated from 9 randomly chosen data
λR (Sys. A)	42.6 %	$\frac{20}{19N_G} \tan [2 (\alpha - \pi/4)]$
λR (Sys. B)	20.0 %	

NOMENCLATURE

a	radius of undeformed drop
\underline{b}	body force, per unit mass
B	length of minor axis of deformed drop
c	concentration of surfactant on the interface
c_s	concentration of surfactant in the bulk phase
D	dimensionless deformation parameter; $(L-B)/(L+B)$
$f(\lambda)$	dimensionless function including dynamic interfacial effects; see Equation (2.2-31)
F	force at the interface necessary to stop all internal circulation
g	gravitational acceleration
G	shear rate of undisturbed shear field
grad γ	interfacial tension gradient
H	curvature
$\underline{j}_A, \hat{j}_A$	bulk phase mass diffusive fluxes of species A, continuous and drop phases
$\underline{j}_A^{(\sigma)}$	interfacial mass diffusive flux of species A
k	interfacial compressibility
L	length of major axis of deformed drop
m	dimensionless circulation number; $TG/4\pi$
n, \hat{n}	refractive indices, continuous and drop phases
$N_{\mathcal{D}}$	dimensionless surfactant diffusion group
N_G	dimensionless capillary number; $\mu Ga/\gamma$
N_{gV}	dimensionless gravitational-viscous number defined by Equation (3.3-1)
N_ϵ	dimensionless interfacial shear viscosity; $\epsilon/\mu a$
N_κ	dimensionless interfacial dilational viscosity; $\kappa/\mu a$

$N_{k+\mathcal{E}}$	dimensionless group; $N_k + N_{\mathcal{E}}$
N_μ	dimensionless viscosity ratio; $\hat{\mu}/\mu$
\underline{P}	interfacial projection tensor
r_0	dimensionless radial position at $\phi = 0$
(r, θ, ϕ)	spherical coordinates
R	dimensionless group defined by Equation (2.2-18)
R_i, R_o	radii of the Couette cylinders, inner and outer
$\underline{S}^{(\sigma)}$	viscous portion of the interfacial stress tensor; see equation (2.1-9)
T	period of circulation
$\underline{\hat{T}}, \underline{\hat{T}}$	bulk phase stress tensors, continuous and drop phases
$\underline{\hat{v}}, \underline{\hat{v}}$	bulk phase velocities, continuous and drop phases
$\underline{v}^{(\sigma)}$	interfacial velocity
V_x, V_y, V_z	velocity components of undisturbed shear field
(x, y, z)	rectangular cartesian coordinates
x^*, y^*	dimensionless x and y
GREEK	
α	orientation angle associated with deformed drop
γ	interfacial tension
γ_{eff}	"effective" interfacial tension defined by Equation (2.2-33)
ϵ	interfacial shear viscosity
ϵ'	dimensionless group defined by Equation (2.2-17)
κ	interfacial dilatational viscosity
κ'	dimensionless group defined by Equation (2.2-16)
λ	dimensionless parameter defined by Equation (2.2-15)
$\hat{\mu}, \mu$	bulk phase viscosities, continuous and drop phases
$\underline{\xi}$	outwardly directed unit normal

$\rho, \hat{\rho}$	bulk phase densities, continuous and drop phases
$\rho^{(\sigma)}$	interfacial density
$\rho_A, \hat{\rho}_A$	bulk phase densities of species A, continuous and drop phases
$\rho_A^{(\sigma)}$	interfacial density of species A
ω_i, ω_o	angular velocities of the Couette cylinders, inner and outer

SYMBOLS

A	subscript denoting species A
$\hat{}$	denotes the drop phase
(σ)	denotes the interface